THE GEOLOGICAL SOCIETY OF AMERICA®

Early Carboniferous ophiolite discovery in central Mongolia: Expanding the record of subduction initiation in the Mongol-Okhotsk Ocean

Mingshuai Zhu[1,2,†], Daniel Pastor-Galán[3,4], Chongrui Tang[1,2], Shun Li[5], Dorjgochoo Sanchir[1,2], Laicheng Miao[1,2], Fuqin Zhang[1,2], Ariuntsetseg Ganbat[6], Munkhtsengel Baatar[7], Chimedtseren Anaad[7], and Jilei Li[1,2,†]

[1]*State Key Laboratory of Lithospheric and Environmental Coevolution, Institute of Geology and Geophysics, Chinese Academy of Sciences, Beijing 100029, China*

[2]*Key Laboratory of Mineral Resources, Institute of Geology and Geophysics, Chinese Academy of Sciences, Beijing 100029, China*

[3]*Instituto de Geociencias, Consejo Superior de Investigaciones Científicas, 28040 Madrid, Spain*

[4]*Frontier Research Institute for Interdisciplinary Sciences, Tohoku University, Sendai 980-8578, Japan*

[5]*School of Oceanography, Shanghai Jiao Tong University, Shanghai 200030, China*

[6]*Department of Mineralogy and Petrology, Georg-August-University Göttingen, 37077 Göttingen, Germany*

[7]*Geoscience Center, Mongolian University of Science and Technology, Ulaanbaatar 120646, Mongolia*

ABSTRACT

The subduction initiation dynamics and southwestern extension of the Mongol-Okhotsk suture zone in Central Asia have been enigmatic due to a scarcity of robust ophiolitic records. This study presents an integrated analysis of petrography, geochemistry, and geochronology conducted on the newly discovered Erdendalai ophiolite in the Dundgobi Province of Mongolia. The ophiolite mainly comprises serpentinized peridotite, gabbro, anorthosite, and chert. Zircon U-Pb dating of an anorthosite sample yields a crystallization age of 350 ± 4 Ma (early Carboniferous), which identifies this ophiolite as the oldest documented ophiolite within the Mongol-Okhotsk Ocean realm. Geochemically, the gabbroic rocks exhibit normal mid-ocean-ridge basalt–like signatures with slight depletion in high field strength elements and enrichment in large ion lithophile elements, resembling forearc basalts. The anorthosites are interpreted to have crystallized from hydrous, arc-related tholeiitic magmas derived from boninitic precursors. These features collectively indicate that the Erdendalai ophiolite formed in a supra-subduction zone setting, specifically an intra-oceanic forearc, during the early Carboniferous. Detrital zircon age spectra from the enclosing Khoidgobi Formation schists show a youngest peak at ca. 302 Ma, constraining the accretion and emplacement of the ophiolite to the latest Carboniferous or later. Our findings not only confirm the southwestern extension of the Mongol-Okhotsk suture but also provide critical evidence for the early Carboniferous subduction initiation of the Mongol-Okhotsk Ocean, likely facilitated by the presence of a continental ribbon rifted during the ocean's opening. The distribution of supra-subduction zone ophiolites with different ages along the Mongol-Okhotsk suture zone may document lateral propagation of subduction initiation.

1. INTRODUCTION

The Central Asian Orogenic Belt (CAOB; Jahn et al., 2000; Windley et al., 2007; also termed the Altaids; Şengör et al., 1993) constitutes one of the largest and longest-lived accretionary collages in the world, with considerable juvenile crustal growth (Jahn et al., 2004; Schulmann and Paterson, 2011; Wang et al., 2023). This giant tectonic domain extends from the Uralides in the west to the Pacific margin in the east and is bounded to the north by the Siberian Craton and to the south by the composite Tarim–North China cratonic blocks (Pirajno et al., 2008; Xiao et al., 2015; Fig. 1A). As the youngest segment of the CAOB, the Mongol-Okhotsk orogenic belt runs northeastward for >3000 km, spanning from the Khangay Mountains in central Mongolia to Uda Bay in the Okhotsk Sea (Figs. 1A and 1B; e.g., Zorin, 1999; Bussien et al., 2011; Tang et al., 2016). Its tectonic evolution is widely attributed to the closure of the Mongol-Okhotsk Ocean (MOO), which separated the Siberian Craton to the north from the Amuri and North China blocks to the south (Tomurtogoo et al., 2005; Van der Voo et al., 2015; Zhu et al., 2023a). The MOO likely closed between the Early–Middle Jurassic and the Early Cretaceous, a process that marked the final stages of crustal amalgamation in East Asia (Van der Voo et al., 2015; Sorokin et al., 2020; Yi and Meert, 2020).

Supra-subduction zone (SSZ) ophiolites, representing fragments of ancient oceanic lithosphere tectonically incorporated into orogenic systems, typically originate during subduction initiation in proto-forearc environments (Pearce, 2003; Dilek and Furnes, 2011; Whattam and Stern, 2011; Stern et al., 2012; van Hinsbergen et al., 2015). Thus, these lithospheric remnants provide critical insights into the mechanisms and geodynamic processes governing subduction nucleation (van Hinsbergen et al., 2015; Guilmette et al., 2018). The spatial-temporal distributions of SSZ ophiolites and numerical modeling indicate that subduction initiations of ancient oceans were more complicated than previously thought, commonly showing significant along-strike variations (Zhou et al., 2018b; Zhu et al., 2024a). In the context of the Mongol-Okhotsk orogenic belt, the Adaatsag ophiolite (ca. 325–319 Ma; Tomurtogoo et al., 2005; Zhu et al., 2023a) and Khuhu Davaa ophiolite (ca. 320 Ma; Zhu et al., 2018) have suggested the subduction of the southwestern MOO initiated during the early Pennsylvanian in the central Mongolia region. However, two major and interrelated knowledge gaps severely limit our understanding of the MOO's subduction system

Mingshuai https://orcid.org/0000-0002-8920-5744

[†]M. Zhu, zhumingshuai@mail.iggcas.ac.cn; J. Li, lijilei@mail.iggcas.ac.cn

GSA Bulletin;
Published online 27 May 2026

https://doi.org/10.1130/B38935.1.

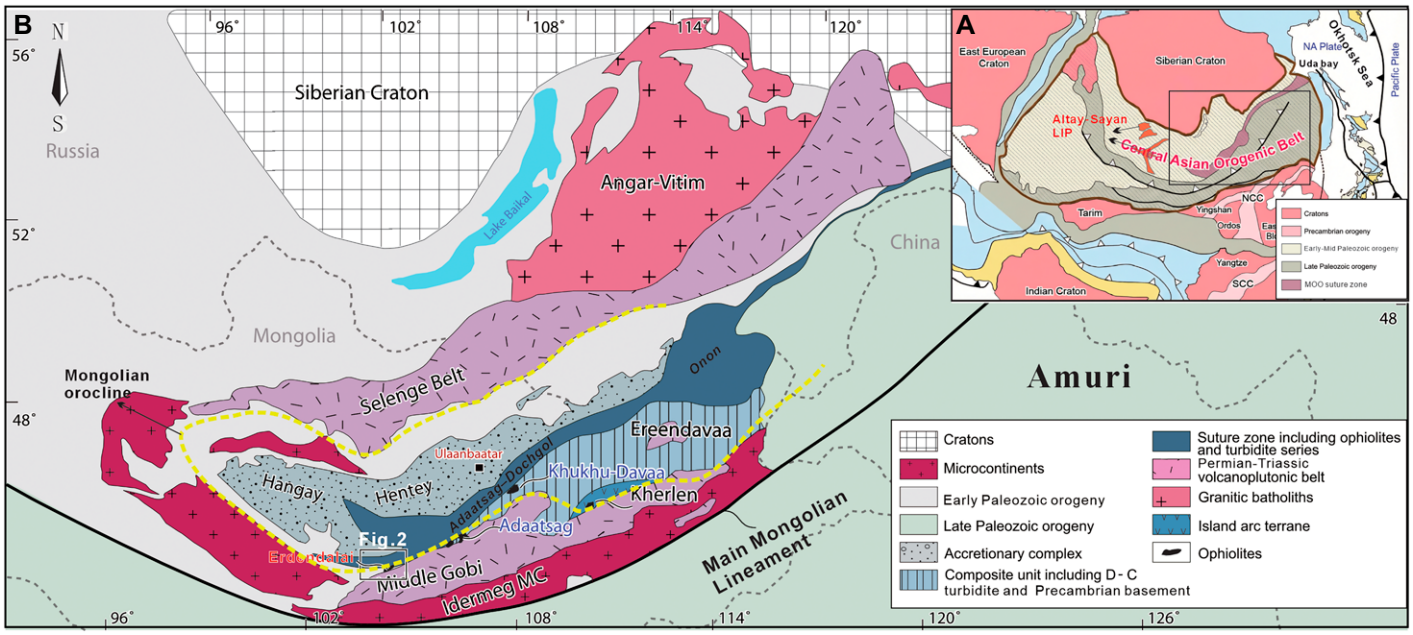

Figure 1. Tectonic map showing the main tectonic units of the Mongol-Okhotsk orogenic belt of central Mongolia (A is modified from Xiao et al., 2015; B is modified from Bussien et al., 2011). NCC—North China Craton; SCC—South China Craton; NA plate—North American plate; LIP—large igneous province; MC—microcontinent; D-C—Devonian–Carboniferous; MOO—Mongol-Okhotsk Ocean.

and, consequently, the evolution of the broader orogen. First, the current documentation of only two SSZ ophiolites within the vast Mongol-Okhotsk orogenic belt is insufficient to characterize such variability or to rigorously test geodynamic models. Second, and closely related, the southwestern continuation of the Mongol-Okhotsk suture zone remains poorly constrained mainly due to the scarcity of robust lithospheric markers such as ophiolites. Consequently, the discovery and comprehensive study of new SSZ ophiolite exposures—particularly in the poorly understood southwestern sector—are imperative. Such work is essential not only to augment the ophiolitic records but also to provide typical markers for the suture zone geometry and better constrain the spatiotemporal pattern of subduction initiation.

To address these critical knowledge gaps, this study focuses on the newly identified early Carboniferous Erdendalai ophiolite, located farther southwest than the previously known Adaatsag and Khuhu Davaa ophiolites. Critically, new zircon U-Pb geochronology suggest the Erdendalai ophiolite formed at ca. 350 Ma, making it ~25–30 m.y. older than these previously documented ophiolites. Combined with petrographic and geochemical data, our results (1) establish the Erdendalai as the oldest known SSZ ophiolite in the Mongol-Okhotsk belt, (2) provide a crucial new lithospheric marker to constrain the southwestern extension of the suture zone, and (3) push back the timing of subduction initiation in the southwestern MOO to the early Carboniferous.

2. GEOLOGICAL SETTING

Mongolia has conventionally been subdivided into two principal tectonic domains along the so-called Main Mongolian Lineament—an approximate regional topographic and structural boundary (Figs. 1A and 1B): a northern domain characterized by early Paleozoic assemblages and a southern domain dominated by late Paleozoic formations (Badarch et al., 2002; Windley et al., 2007). The northern domain comprises Archean–Proterozoic microcontinental fragments, Neoproterozoic to Lower Paleozoic metamorphic units and ophiolitic sequences, and Paleozoic volcanic and sedimentary cover. The recently-identified >1000-km-long eclogite-bearing Cambrian high-pressure metamorphic belt (ca. 548–520 Ma) in west Mongolia and the >1000-km-long granulite-bearing metamorphic belt at the southern margin of the Siberian craton (507–490 Ma) provide robust evidence for major early Paleozoic orogenesis during the Cambrian (Gladkochub et al., 2008; Zhu et al., 2023b). In contrast, the southern domain is primarily composed of lower to middle Paleozoic ophiolites, together with arc-derived volcanic and volcaniclastic rocks (e.g., Badarch et al., 2002). The northern domain is transected by the younger Mongol-Okhotsk orogenic belt, a feature linked to the subduction and final closure of the MOO (Parfenov et al., 2001; Bussien et al., 2011; Donskaya et al., 2013; Fig. 1). Interpretations regarding the origin of the MOO vary among previous studies, which have attributed it to an Ediacaran–Cambrian ocean situated between the Siberian Craton and the Tuva-Mongol massif (Şengör et al., 1993), an early Carboniferous–earliest Permian embayment of the Paleo-Pacific Ocean (Zorin, 1999), or a Late Ordovician–Silurian ocean formed by backarc extension of the Paleo-Asian Ocean (Bussien et al., 2011; Domeier, 2018). Recent investigations have identified a bimodal volcanic suite (415–410 Ma) and coeval volcanic-sedimentary sequences in northwestern Mongolia, which constitute part of the Altay-Sayan Large Igneous Province (Zhu et al., 2024b). These findings support a model in which an Early Devonian mantle plume impacted and thermally eroded the lithosphere of the early Paleozoic collage in the CAOB, ultimately leading to the opening of the MOO (Zhu et al., 2024b). The Mongol-Okhotsk orogenic belt overall formed as an orocline during the closure of the MOO, as evidenced by the concentric horseshoe-shaped microcontinental ribbons and magmatic arcs, along with a distinctive U-shaped aeromagnetic signature (Xiao et al., 2018; Wang et al., 2022). Subduction of the MOO initiated in the Pennsylvanian (Zhu et al., 2023a), with oceanic lithosphere being

consumed through bidirectional subduction—southward beneath the Amur Block and northward beneath the Siberian Craton (Donskaya et al., 2013; Tang et al., 2016; Liu et al., 2018; Wang et al., 2022). Based on the tectonic terrane framework established by Badarch et al. (2002), the study area is situated near the boundary separating the Hangay-Hentey belt to the north from the Middle Gobi volcano-plutonic belt to the south.

Superimposed upon the older early Paleozoic tectonic framework, the Hangay-Hentey belt (Fig. 1) constitutes a major part of the younger Mongol-Okhotsk orogenic belt. It is predominantly composed of Silurian to Carboniferous turbidites intruded by numerous late Paleozoic to early Mesozoic granitoids (Badarch et al., 2002; Bussien et al., 2011; Ganbat et al., 2021). The Silurian–Devonian strata are characterized by pelagic red radiolarian chert beds and deep-sea turbidites intercalated with ocean-island basalt–type mafic volcanic rocks. In contrast, the Carboniferous units exhibit a shallowing-upward succession, transitioning from turbiditic deposits to proximal deltaic facies (Kelty et al., 2008; Kurihara et al., 2009; Bussien et al., 2011). Detrital zircon geochronology of the Paleozoic sedimentary rocks reveals dominant age peaks in the Mississippian (Kelty et al., 2008) and/or Devonian (Bussien et al., 2011). The Hangay-Hentey belt has been widely interpreted as a Devonian–Carboniferous accretionary wedge of the MOO (Kurihara et al., 2009; Bussien et al., 2011).

The Middle Gobi belt is dominated by Carboniferous–Triassic calc-alkaline volcanic and plutonic rocks, interpreted to record the southward subduction of the MOO (e.g., Badarch et al., 2002; Tomurtogoo et al., 2005; Zhao et al., 2017). Its basement consists of the Ereendavaa terrane—a microcontinent with a Paleoproterozoic crystalline basement overlain by Neoproterozoic metasedimentary and metavolcanic units (Bold et al., 2025). Early–middle Paleozoic gneisses, amphibolites, and schists in the region are inferred to reflect the evolution of the Kherlen Ocean, as supported by the presence of the Kherlen ophiolite (ca. 566–510 Ma; Miao et al., 2016, 2017; Narantsetseg et al., 2019). Post-collisional granites emplaced at ca. 440 Ma indicate that the closure of the Kherlen Ocean occurred prior to the Silurian, resulting in the amalgamation of the Ereendavaa and Idermeg continental terranes (Miao et al., 2016). These combined terranes subsequently formed the southern continental margin of the MOO. Furthermore, Late Permian backarc ophiolites and Triassic bimodal volcanic suites identified south of the Middle Gobi belt imply multiple phases of backarc extension during the continued southward subduction of the MOO (Zhu et al., 2016, 2023c).

3. GEOLOGY AND PETROGRAPHY OF THE ERDENDALAI OPHIOLITE

The newly discovered ophiolite, designated as the Erdendalai ophiolite, is located ~50 km west of Erdendalai village in Dundgobi Province, Mongolia (Fig. 2). It crops out as tectonic lenses (up to 0.5 km along-strike length and 0.1 km in apparent thickness) within the volcano-sedimentary Khoidgobi Formation that exhibits a well-developed foliation striking ~155° and dipping 30° to the southwest (Fig. 2). The ophiolitic slices mainly comprise serpentinized peridotite, pyroxenite, gabbro, anorthosites, and chert (Fig. 3). The anorthosites occur as centimeter- to decimeter-thick layers or lenses in the serpentinized peridotite (Figs. 3A and 3C). Although the Khoidgobi Formation is regionally described as consisting of mica schist, quartz-amphibole and biotite-amphibole schist, marble and green schist, and has experienced greenschist-to-amphibolite facies metamorphism and varying degrees of deformation (Jamyandorj et al., 1990), our field observations within the study area specifically identified micaschist (Fig. 3F). Although previously attributed to the Precambrian (Jamyandorj et al., 1990), no isotopic ages have been reported to confirm this assignment.

The peridotites exhibit extensive serpentinization, with olivine and orthopyroxene being either completely or partially replaced by serpentine minerals (Fig. 4A). Modal mineralogy estimates indicate that the peridotite consists of ~80% serpentine, 10% magnetite, 5% olivine, and 5% orthopyroxene. The gabbro displays a medium- to coarse-grained poikilitic texture (Fig. 4B) and is predominantly composed of hornblende (~50%), plagioclase (~40%), and pyroxene (~10%). Anorthosites are characterized by fine-grained calcic plagioclase making up ~95% of the rock and a minimal mafic component (hornblende ~5%; Fig. 4C). A representative schist sample from the Khoidgobi Formation contains ~40% quartz and 50% plagioclase, both aligned within the foliation plane, along with ~5% magnetite and 5% lithic fragments (containing some relict hornblende and feldspar assemblages characteristic of igneous rocks; Fig. 4D).

4. ANALYTICAL METHODS

4.1. Geochemistry

Whole-rock major and trace element compositions were determined at the Wuhan Sample Solution Analytical Technology Co., Ltd., China by X-ray fluorescence (XRF) and inductively coupled plasma–mass spectrometry (ICP-MS). The precision of the XRF analyses is within ±2% for the oxides >0.5 wt% and within ±5% for the oxides >0.1 wt%. Analytical results for U.S. Geological Survey standards indicated that the data are accurate within ±5% for the trace elements.

4.2. Zircon U-Pb Geochronology

Zircon crystals were extracted from crushed rocks using conventional heavy liquid and magnetic separation techniques and hand-picked under a binocular microscope. The zircons were mounted in epoxy resin and polished to expose the grain centers. Optical (transmitted and reflected light) photographs and cathodoluminescence (CL) images were prepared to reveal the internal texture of the zircons in order to select optimal sites for analysis. Finally, the mounts were vacuum-coated with high-purity gold.

Zircon U-Pb dating for magmatic rocks using the sensitive high-resolution ion microprobe (SHRIMP) secondary ionization mass spectrometry instrument was carried out at the Beijing SHRIMP Center, Institute of Geology, Chinese Academy of Geosciences, following the standard procedures described by Jian et al. (2012). The spot size of the ion beam was ~20 μm and analytical data for individual spots are the mean values of five consecutive analyses. The analytical data were processed using the software programs Squid 1.03 (Ludwig, 2001) and Isoplot 3.0 (Ludwig, 2003). Errors of individual analyses are given at the two standard deviation level and the ages reported in the paper are weighted mean $^{206}Pb/^{238}U$ ages with common Pb correction using the ^{204}Pb-based methods of Compston et al. (1984).

Detrital zircon U-Pb dating for sedimentary rocks by laser ablation (LA)-ICP-MS was conducted at Beijing GeoAnalysis Co., Ltd. Pre-ablation was conducted for each spot analysis using five laser shots to remove potential surface contamination. The analysis was performed using a 30 μm diameter spot. The Iolite software package was used for data reduction (Paton et al., 2010). Zircon 91500 was used as the primary reference material, whereas zircon GJ-1 (609 Ma; Jackson et al., 2004) and Plešovice (337 Ma; Sláma et al., 2008) were used to check accuracy. Typically, 35–40 seconds of the sample signals were acquired after 20 seconds of gas background measurement. The exponential function was used to calibrate the downhole fractionation (Paton et al., 2010). The analyses yielded weighted mean $^{206}Pb/^{238}U$ ages of 606 ± 4 Ma for GJ-1 and 338 ± 2 Ma for Plešovice, which agree with the reference values.

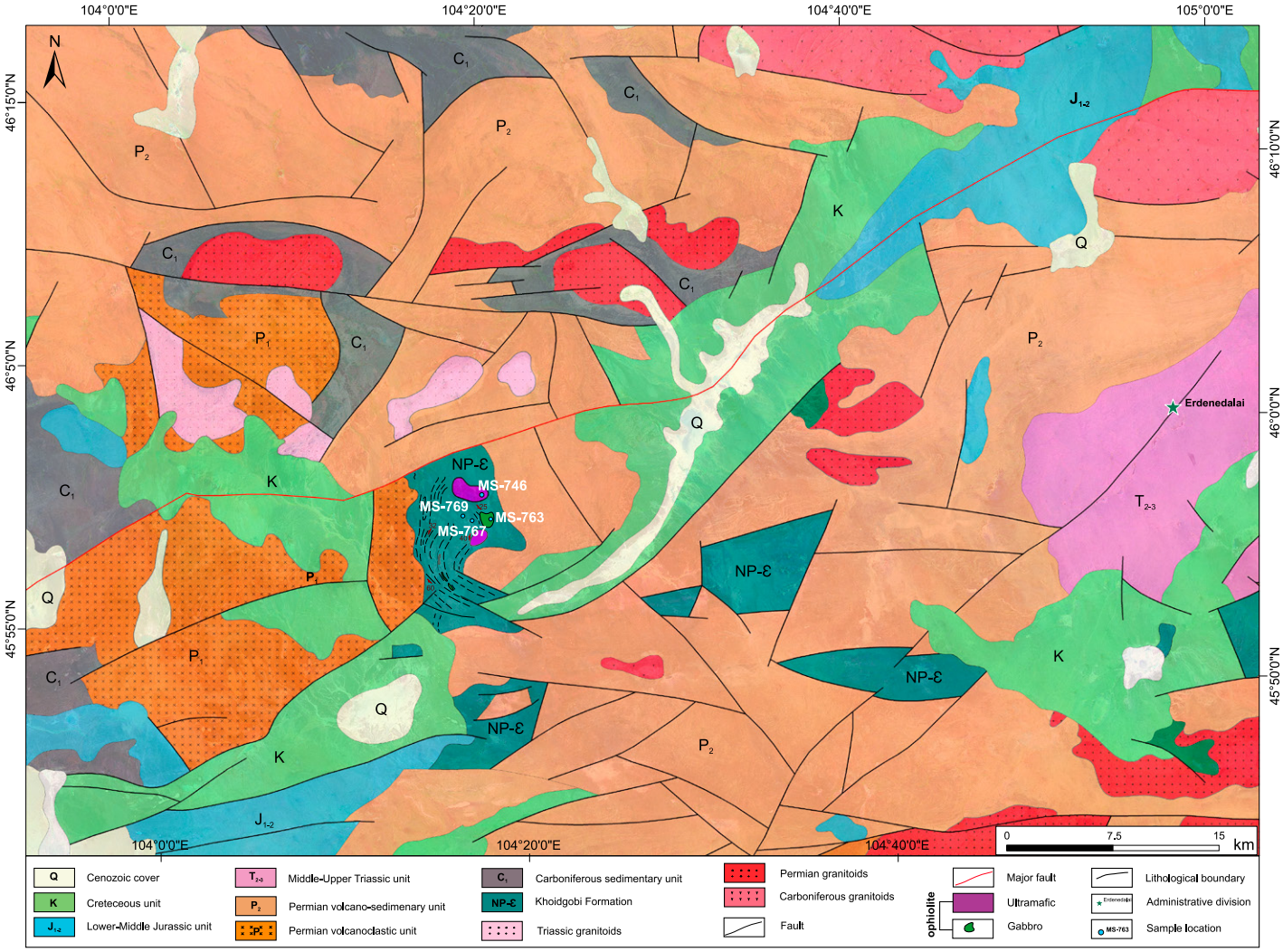

Figure 2. Regional geologic map of the Erdendalai ophiolite study area in central Mongolia (modified from Zabotkin et al., 1982; Jamyandorj et al., 1990; and Erdenechimeg and Enkhabayar, 2017).

5. RESULTS

5.1. Whole-Rock Major and Trace Elements

Major and trace element compositions for ten samples from the Erdendalai ophiolite—comprising one ultramafic sample, six gabbros, and three anorthosites—are provided in Table S1 in the Supplemental Material.[1] Although fresh samples were carefully selected for analysis, the ultramafic rock has high loss-on-ignition (LOI) values (11.80 wt%), indicating variable degrees of alteration. The ultramafic rock is characterized by low SiO_2 (41.28 wt%) and alkalinity ($Na_2O + K_2O$) contents (0.03 wt%), and high MgO (36.87 wt%) and $Fe_2O_3^T$ contents (7.79 wt%), with Mg# [= molar Mg/(Mg + Fe^{2+})] of 0.92. The ultramafic sample has low total rare earth element (REE) contents (13.84 ppm) and the incompatible mantle trace elements such as Rb, Nb, and Ta are depleted. In contrast, concentrations of mantle compatible elements such as Cr (3324 ppm) and Ni (1937 ppm) are extremely high in the sample.

The gabbro samples exhibit variable SiO_2 (45.36–52.75 wt%), MgO (4.09–10.76 wt%), CaO (10.09–15.84 wt%), Al_2O_3 (12.03–20.33 wt%), Na_2O (0.77–4.68 wt%), and TiO_2 (0.28–1.36 wt%) contents, but low K_2O (0.03–0.21 wt%) and P_2O_5 (0.02–0.12 wt%) contents. Mg# values range from 0.64 to 0.77. The samples have REE contents between 11.49 ppm and 49.42 ppm with no or positive Eu anomalies (Eu/Eu* = 0.89–2.64). With the exception of sample MS-753-2, all gabbros exhibit distinct chondrite-normalized light REE (LREE) depletion (La_N/Yb_N = 0.56–1.17; Fig. 5A). In a primitive mantle–normalized trace element variation diagram, most gabbro samples are enriched in large ion lithophile elements (LILEs; e.g., Sr, Ba, and U) and slightly depleted in high field strength elements (HFSEs; e.g., Nb, Ta, and Ti; Fig. 5B).

The anorthosite samples have low SiO_2 (49.99–52.57 wt%), MgO (0.41–0.67 wt%), $Fe_2O_3^T$ (0.42–0.62 wt%), and K_2O (0.05–0.09 wt%) contents, but have high CaO (12.46–14.20 wt%) and Al_2O_3 (23.94–26.00 wt%) contents. The samples show REE contents of

[1]Supplemental Material. Table S1: Whole-rock compositions of various rocks from the Erdendalai ophiolite. Table S2: SHRIMP zircon U-Pb analytical data for the anorthosite from the Erdendalai ophiolite. Table S3: LA-ICP-MS zircon U-Pb analytical data for the schist from the Khoidgobi Formation. Table S4: Compilation of detrital zircon ages of the Late Paleozoic–Mesozoic accretionary complexes from the southwest segment of the Mongol-Okhotsk orogenic belt. Please visit https://doi.org/10.1130/GSAB.S.32293206 to access the supplemental material; contact editing@geosociety.org with any questions.

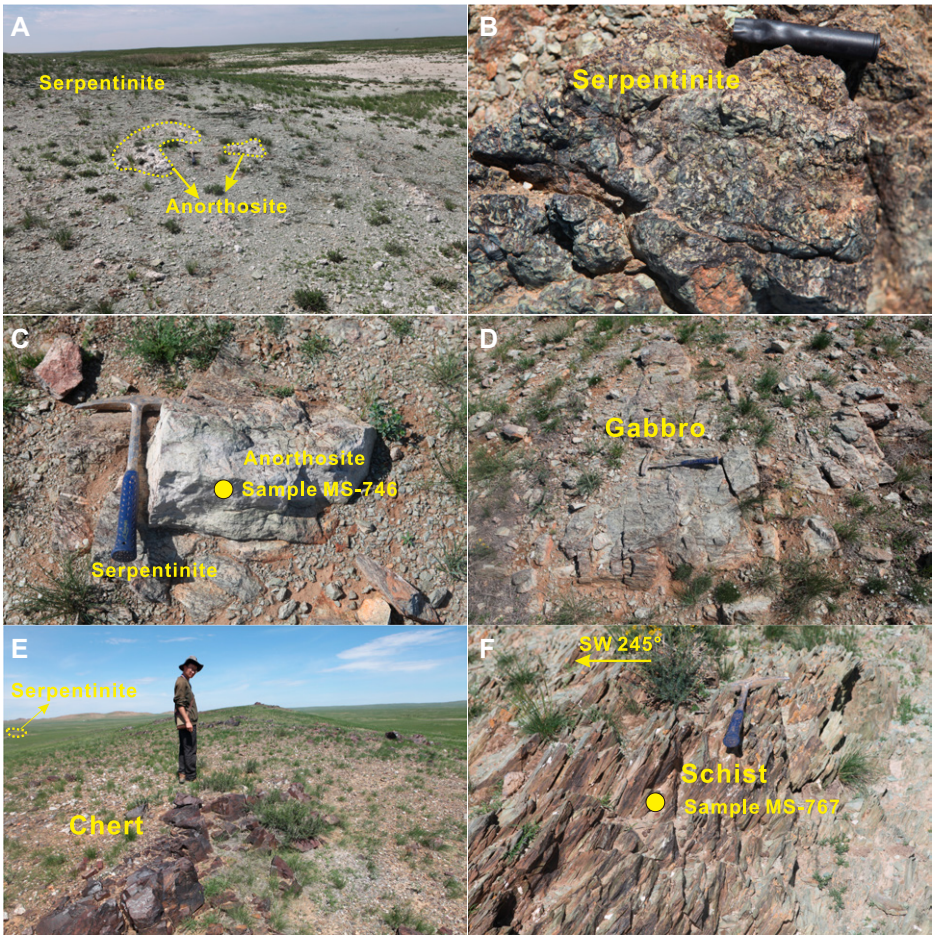

Figure 3. Field photographs showing the occurrences of the Erdendalai ophiolite and the associated Khoidgobi Formation in central Mongolia. (A) Serpentinized ultramafic rocks with anorthosites layers or lenses. (B) Serpentinized ultramafic rocks displaying a mesh texture. (C) Anorthosites occur as lenses in the serpentinized ultramafic rocks. (D) Gabbro fragments within the schist of the Khoidgobi Formation. (E) Red chert occurs as tectonic blocks in fault contact with ultramafic rocks. (F) Schist of the Khoidgobi Formation characterized by a well-developed foliation (dipping 30° to the southwest).

16–52 ppm and the chondrite-normalized REE patterns of the samples are slightly fractionated and exhibit distinct chondrite-normalized LREE depletion [$(La/Yb)_N = 0.25–0.31$)] and positive Eu anomalies (Eu/Eu* = 1.33–1.48; Fig. 5C). They exhibit negative Nb and Ti anomalies but slightly positive Zr, Hf, and Sr anomalies in primitive mantle–normalized trace element diagrams (Fig. 5D).

5.2. Zircon U-Pb Geochronology

One anorthosite sample from the Erdendalai ophiolite and two schist samples from the Khoidgobi Formation were selected for SHRIMP U-Pb zircon dating and LA-ICP-MS U-Pb detrital zircon dating, respectively. The analytical results are presented in Tables S2 and S3.

Zircons extracted from the anorthosite sample MS-746 collected from the Erdendalai ophiolite are euhedral to subhedral prisms measuring 75–150 μm in length. Most grains display well-defined oscillatory zoning (Fig. 6A), a feature typical of magmatic zircon (e.g., Rubatto, 2002). Twelve zircon grains were analyzed, showing U concentrations ranging from 25 ppm to 425 ppm and Th concentrations ranging from 21 ppm to 215 ppm. Th/U ratios vary between 0.35 and 1.11, consistent with an igneous origin (Rubatto, 2002). Eight analyses yielded a weighted mean $^{206}Pb/^{238}U$ age of 350 ± 6 Ma (mean square of weighted deviates = 0.86; Fig. 6B), which is interpreted as the crystallization time of the zircons. One spot analysis yielded an older age of ca. 2522 Ma, likely reflecting zircon inheritance. The remaining three zircons yielded much younger ages (269–241 Ma), which are interpreted to be the result of disturbance or resetting of zircons during a later tectono-thermal event.

Detrital zircons separated from the schist sample MS-767, collected from the Khoidgobi Formation, exhibit rounded to subhedral morphologies and range from 50 μm to 200 μm in size. CL imaging reveals that most grains have oscillatory or planar-banded growth zones (Fig. 6A), indicating a magmatic origin (Rubatto, 2002). A total of 60 U-Pb analyses were obtained, and they have U contents ranging from 24 ppm to 803 ppm and Th contents ranging from 14 ppm to 1143 ppm, and Th/U ratios ranging from 0.28 to 1.42. All the analyses yielded ages ranging from 2361 ± 56 Ma to 324 ± 4 Ma, which cluster in four main age groups: (1) U-Pb ages of 345–324 Ma, with a peak at 334 Ma; (2) 371–347 Ma, with a peak at 357 Ma; (3) 394–375 Ma, with a peak at 385 Ma; and (4) 418–402 Ma, with a minor peak at 410 Ma (Figs. 6C and 6D).

Detrital zircons from the schist sample MS-769 collected from the Khoidgobi Formation are rounded to subhedral and range from 100 μm to 200 μm in size. CL imaging reveals that most grains have oscillatory or planar-banded growth zones (Fig. 6A), indicating a magmatic origin (Rubatto, 2002). Sixty U-Pb analyses indicate U concentrations of 18–799 ppm, Th concentrations of 18–955 ppm, and Th/U ratios ranging from 0.69 to 1.20. The obtained $^{206}Pb/^{238}U$ ages vary from 769 ± 7 Ma to 300 ± 5 Ma and define four principal age clusters: (1) U-Pb ages of 304–300 Ma, with a minor peak at 302 Ma; (2) 340–314 Ma, with a peak at 328 Ma; (3) 395–342 Ma, with a peak at 365 Ma; and (4) 439–437 Ma, with a minor peak at 438 Ma (Figs. 6E and 6F).

6. DISCUSSION

6.1. Ages of the Erdendalai Ophiolite and Associated Sedimentary Rocks

The Erdendalai ophiolite had not been recognized in previous studies and the associated Khoidgobi Formation was ascribed to the Riphean sequence on an earlier geological map (Jamyandorj et al., 1990) and to Permian sedimentary units on a later map (Li et al., 2008). Consequently, no isotopic dating data has yet been reported for the Erdendalai ophiolite. The anorthosite from the ophiolite yielded a SHRIMP zircon U-Pb concordant age of 350 ± 4 Ma, which is interpreted to represent the crystallization ages of the anorthosite based on the magmatic signature of the analyzed zircons (oscillatory zoning in CL images and high Th/U ratios

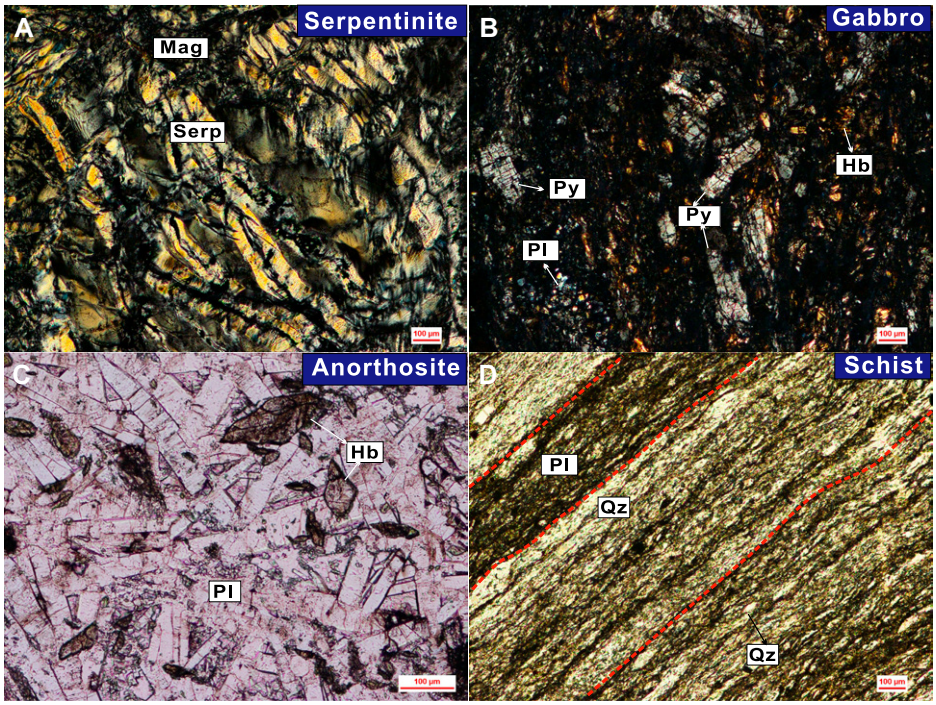

Figure 4. Microphotographs of the Erdendalai ophiolite and the samples from central Mongolia used for age dating. (A) Ultramafic rocks with strong serpentinization. (B) Gabbro with a poikilitic texture. (C) Anorthosites from the Erdendalai ophiolite. (D) Schist from the Khoidgobi Formation, with red dashed lines outlining the primary foliation plane. Serp—serpentine; Mag, magnetite; Py—Pyroxene; Hb—hornblende; Pl—plagioclase, Qz—quartz.

because of the preferential incorporation of Th over U during melt crystallization). This robust geochronological result constrains the formation of the Erdendalai ophiolite to the early Carboniferous. Notably, this unit represents the oldest known ophiolite along the Mongol-Okhotsk orogenic belt, implying that the MOO had already initiated rifting and oceanic crust formation prior to the early Carboniferous. The presence of older inherited zircon grains within the anorthosite may originate from entrained crustal fragments, delaminated continental lithosphere during ocean opening, or continental material incorporated along transform faults and mid-ocean ridge systems (Pilot et al., 1998).

The two schist samples (MS-767 and MS-769) from the Khoidgobi Formation, which encloses the Erdendalai ophiolite, exhibit a broad spectrum of detrital zircon U-Pb ages. A significant proportion of these ages fall within the 400–320 Ma range, consistent with age distributions documented from late Paleozoic to Mesozoic accretionary complexes adjacent to the Mongol-Okhotsk suture zone (Fig. 7; Table S4; Kelty et al., 2008; Bussien et al., 2011; Hara et al., 2013; Ruppen et al., 2014). These metasedimentary rocks, interleaved with ophiolitic slices, are interpreted as components of a subduction-accretionary complex. In such tectonic settings, the detrital zircons are likely derived from nearby magmatic arcs and rapidly deposited into adjacent forearc or trench basins, and the age of the youngest zircon population provides a maximum estimate for the timing of sediment deposition. The presence of a prominent youngest zircon peak at ca. 302 Ma suggests that the Khoidgobi Formation was deposited after the latest Carboniferous—rather than in the Precambrian as previously proposed.

The southwestern segment of the Mongol-Okhotsk suture zone is manifested as the Adaatsag-Dochgol terrane, which correlates with the Onon terrane in its northeastern Russian extension (Fig. 1; Parfenov et al., 2001; Badarch et al., 2002; Zhu et al., 2023a). The Dochgol terrane contains deformed and metamorphosed Devonian to Triassic marine sandstone, shale, conglomerate, and minor volcanic rocks (Badarch et al., 2002; Bussien et al., 2011). The Adaatsag terrane is predominantly composed of intensely deformed schist, quartzite, metasandstone, phyllite, chert, metavolcanic rocks, limestone, mélange, and dismembered ophiolitic fragments, all of which have undergone greenschist- to amphibolite-facies metamorphism (Parfenov et al., 2001; Badarch et al., 2002). As noted in previous sections, the southwestern continuation of this suture has remained poorly constrained, largely due to insufficient documentation of ophiolitic remnants within this segment. The identification of the Erdendalai ophiolite and its associated Carboniferous metasedimentary rocks in this study provides critical evidence supporting the southwestern extension of the Mongol-Okhotsk suture zone, thereby helping to clarify the regional tectonic architecture.

6.2. Petrogenesis and Tectonic Setting

Petrographic and geochemical analyses indicate that the studied samples underwent varying degrees of hydrothermal alteration. However, no systematic correlation was observed between LOI values and key major element oxides such as SiO_2, TiO_2, and Na_2O (Figs. 8A–8D), indicating that these elements remained largely immobile during alteration processes (Nakamura et al., 2007). Zirconium (Zr), known for its low mobility under hydrothermal conditions, was employed as a reference element to assess the behavior of other trace elements (Pearce, 2014). Elements including Nb, La, and Yb exhibit well-constrained linear correlations with Zr, confirming their immobile nature, whereas others such as Rb and Pb display significant scatter due to their post-magmatic mobility (Figs. 8C–8F). These relationships support the interpretation that the samples have largely retained their primary magmatic geochemical signatures.

Although mantle-derived magmas are commonly subject to crustal contamination during ascent, several lines of geochemical evidence argue against significant assimilation in the studied samples. The absence of correlation between Nb/La and Th/La ratios with SiO_2, combined with low Th/Ce (0.01–0.03) and Th/La (0.02–0.06) values, indicates negligible crustal contamination in the gabbros (Figs. 9A and 9B). Similarly, Th/Ta ratios in the gabbros range from 0.79 to 3.12, closely matching the primitive mantle value (Th/Ta = ~2.3) and contrasting sharply with typical continental crust (Th/Ta = ~10), further supporting a lack of crustal input (Sun and McDonough, 1989). The gabbroic samples exhibit lower Mg# (0.65–0.77), Cr (82–629 ppm), and Ni (51–232 ppm) than expected for primitive mantle melts (Mg# values of 0.68–0.76, Cr contents of 300–500 ppm and Ni contents of 300–400 ppm; Frey et al., 1978; Wilson, 1989), consistent with an evolved magmatic origin. Positive correlations between Cr and Ni with Mg# in the gabbros suggest

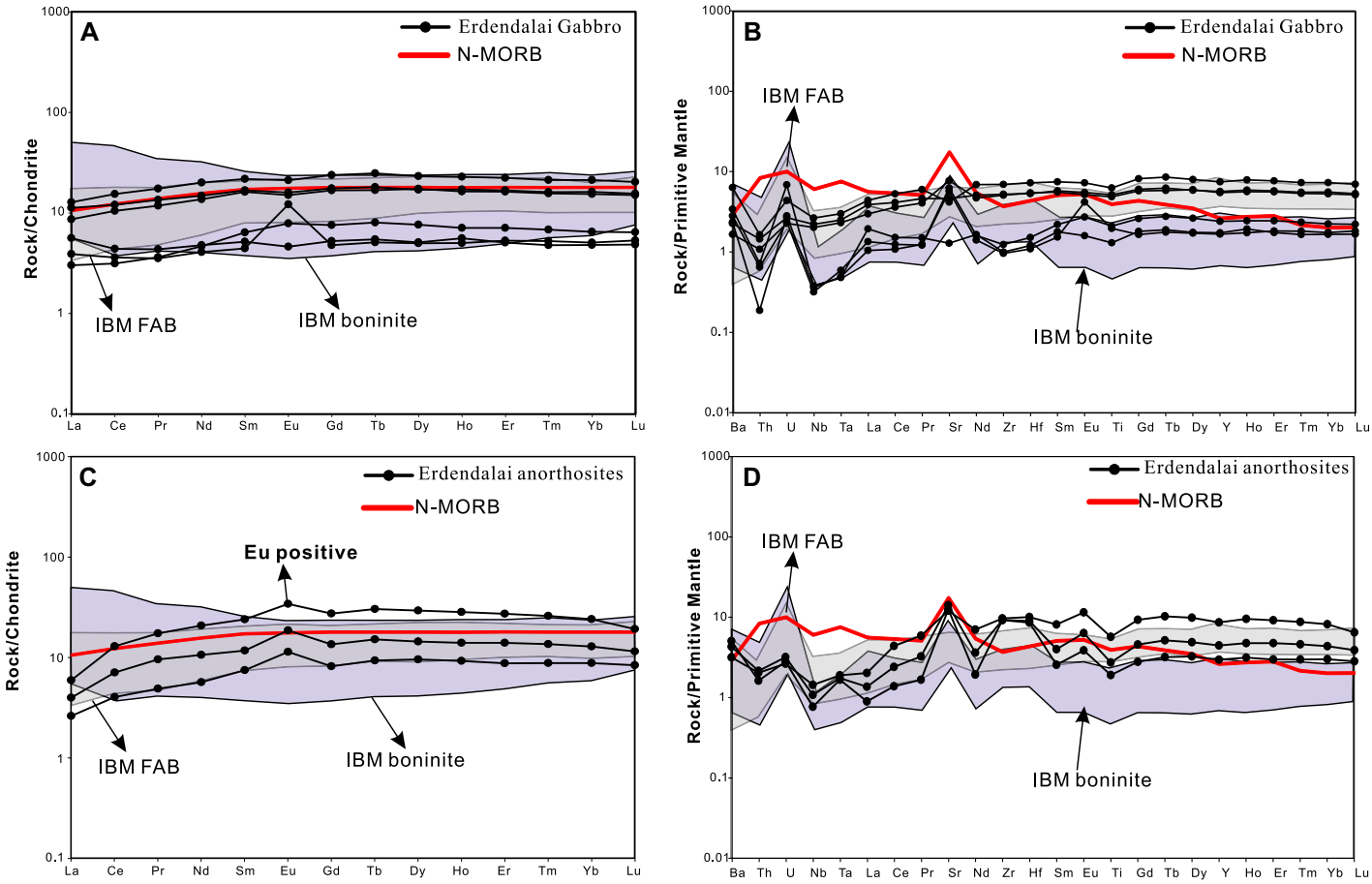

Figure 5. Chondrite-normalized rare earth element patterns and primitive mantle–normalized diagrams for the Erdendalai ophiolite from central Mongolia. (A, B) Gabbros. (C, D) Anorthosites. Normalizing values are from Sun and McDonough (1989). Data sources of Izu–Bonin–Mariana forearc basalts (IBM-FAB) are from Reagan et al. (2010), data sources of IBM boninite are from Ishizuka et al. (2020) and Shervais et al. (2021). N-MORB—normal mid-ocean-ridge basalt.

fractional crystallization of olivine and clinopyroxene (Figs. 9C and 9D), because Cr and Ni are strongly compatible in these minerals (Cr in clinopyroxene/spinel, Ni in olivine) and are therefore efficiently removed together with Mg during crystallization (Wilson, 1989; Rollinson, 1993). Partition coefficient-based discrimination using Ni-Cr and V-Cr relationships (Rollinson, 1993) points to clinopyroxene—rather than olivine or hornblende—as the dominant fractionating phase (Figs. 9E and 9F). The absence of a correlation between Dy/Yb and SiO_2 (Fig. 9G) argues against significant amphibole fractionation (Davidson et al., 2007). Positive Eu anomalies in some gabbros indicate plagioclase accumulation, because Eu occurring significantly as Eu^{2+} in magmatic systems could substitute readily for Ca in plagioclase. This causes plagioclase to strongly partition Eu relative to trivalent REEs, so that plagioclase accumulation imparts a positive Eu anomaly to the whole-rock composition (Drake and Weill, 1975; Aigner-Torres et al., 2007). The lack of correlation between TiO_2 and MgO suggests limited fractionation of Fe-Ti oxides (e.g., ilmenite and magnetite) during magma differentiation (Fig. 9H), because in magmatic systems where Fe-Ti oxides crystallize and are removed, they efficiently scavenge TiO_2 from the melt, typically generating a positive correlation between decreasing TiO_2 and decreasing MgO (Wilson, 1989; Rollinson, 1993).

The gabbroic rocks from the Erdendalai ophiolite exhibit geochemical signatures typical of normal mid-ocean-ridge basalts (N-MORBs), suggesting derivation from a depleted mantle source (Sun and McDonough, 1989). Our interpretation is supported by multiple tectono-magmatic discrimination diagrams (Figs. 10A–10D). However, compared to typical N-MORB, the gabbros display lower concentrations of HFSEs, such as Nb and Ta, a feature more consistent with forearc basalts (FABs; Figs. 5A and 5B; Reagan et al., 2010; Ishizuka et al., 2011; Hickey-Vargas et al., 2018). They also show mild enrichment in LILEs (e.g., Ba and U), indicative of contributions from slab-derived fluids or melts (Stern, 2002; Ishizuka et al., 2014). This interpretation is further supported by the Nb/Yb versus Th/Yb diagram, in which several gabbro samples plot slightly above the mantle array (Fig. 10A). In the Nb_N-Th_N discrimination diagram (Saccani, 2015), most samples fall near the boundary between the N-MORB and FABs fields (Fig. 10C). In the Nb-Zr-Y diagram (Meschede, 1986), all the gabbro samples plot in the island-arc basalt/N-MORB field (Fig. 10D). The overall geochemical character—marked by HFSE depletion and LILE enrichment—is indicative of arc-related magmatism. We therefore propose that the Erdendalai ophiolite likely formed in an intra-oceanic forearc setting.

Anorthosite can constitute a petrogenetically significant component within ophiolitic sequences despite that they are volumetrically

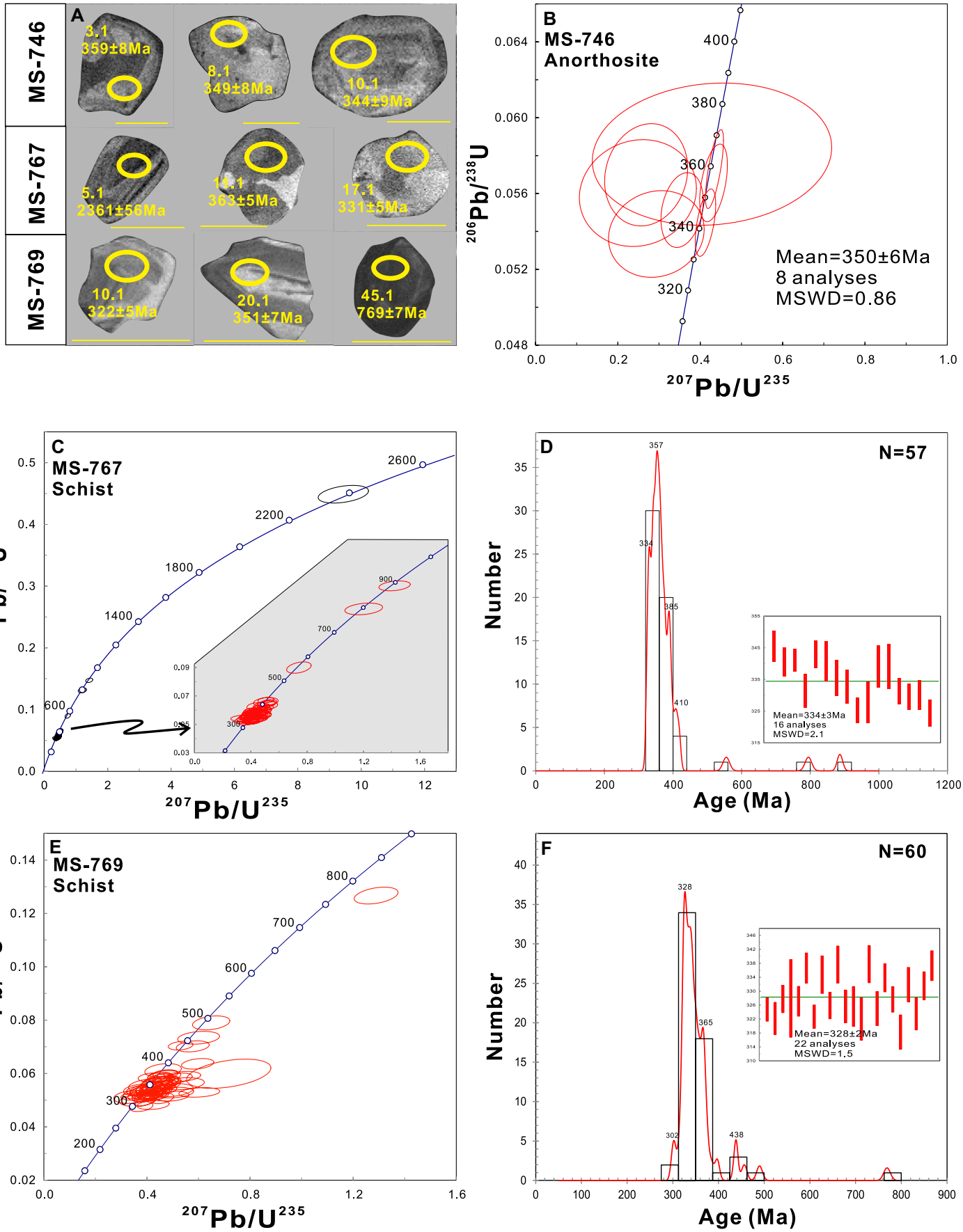

Figure 6. Representative cathodoluminescence (CL) images of zircons and zircon U-Pb concordia diagrams for the Erdendalai ophiolite and the associated Khoidgobi Formation from central Mongolia. (A) Representative CL images of analyzed zircons. Yellow circles represent sites of analytical spots and the numbers around the circles are the spot numbers and ages. (B) U-Pb concordia diagram for the anorthosite. (C, D) Detrital zircon U-Pb concordia and relative probability diagrams for sample MS-767 schist from the Khoidgobi Formation. (E, F) Detrital zircon U-Pb concordia and relative probability diagrams for sample MS-769 schist from the Khoidgobi Formation. MSWD—mean square of weighted deviates; N—number.

small. Anorthosite-bearing ophiolites generally possess tholeiitic affinity exhibiting low La/Nb, Th/Nb, La/Yb and Th/Yb ratios, along with trace element patterns resembling N-MORB (Ross and Bédard, 2009; Dilek and Furnes, 2009; Saccani, 2015; Golowin et al., 2017). Formed in oceanic settings and emplaced into oceanic crust, these anorthosites are typically uncontaminated by continental material, making them reliable indicators of mantle source characteristics and tectonic environments (Sotiriou and Polat, 2020, 2023). A comprehensive compilation of Tethyan anorthosite-bearing ophiolites indicates that these anorthosites predominantly derived from tholeiitic magmas in subduction-related settings, although some also occur in mid-ocean ridges, continental rifts, and mantle plume environments (Takagi et al., 2005; Piccardo and Guarnieri, 2011; Sotiriou and Polat, 2020). The anorthosites within the Erdendalai ophiolite display negative Nb and Ti anomalies, N-MORB trace element characteristics and elevated CaO concentrations, and are spatially associated with gabbros exhibiting subduction-related geochemical signatures (Fig. 5). These features collectively indicate the anorthosites in this study crystallized from hydrous, arc-related tholeiitic magmas within a subduction zone setting. A significant number of Phanerozoic anorthosites in subduction zone are interpreted to have originated from boninitic parental magmas, which themselves formed through high-degree partial melting of highly depleted, hydrous mantle sources that had been metasomatized by slab-derived fluids and melts (Golowin et al., 2017; Woelki et al., 2018; Sotiriou and Polat, 2020, 2023). Since boninitic magmas are typically plagioclase-undersaturated (Crawford, 1989), they likely experienced extensive fractional crystallization of olivine and pyroxene at depth, evolving into hydrous, calcium- and aluminum-enriched tholeiitic melts. Consequently, the anorthosites did not crystallize directly from boninitic melts, but rather from these more differentiated tholeiitic magmas derived from boninitic precursors (Sotiriou and Polat, 2020, 2023). The involvement of boninitic magmas to anorthosite petrogenesis suggests that these rocks formed during the initial phases of subduction zone development, most likely within a forearc tectonic setting (Dilek and Furnes, 2009; Reagan et al., 2010; Hickey-Vargas et al., 2018).

The Carboniferous Erdendalai ophiolite and its associated sediments are located in the southernmost part of the Hangay-Hentey belt—a

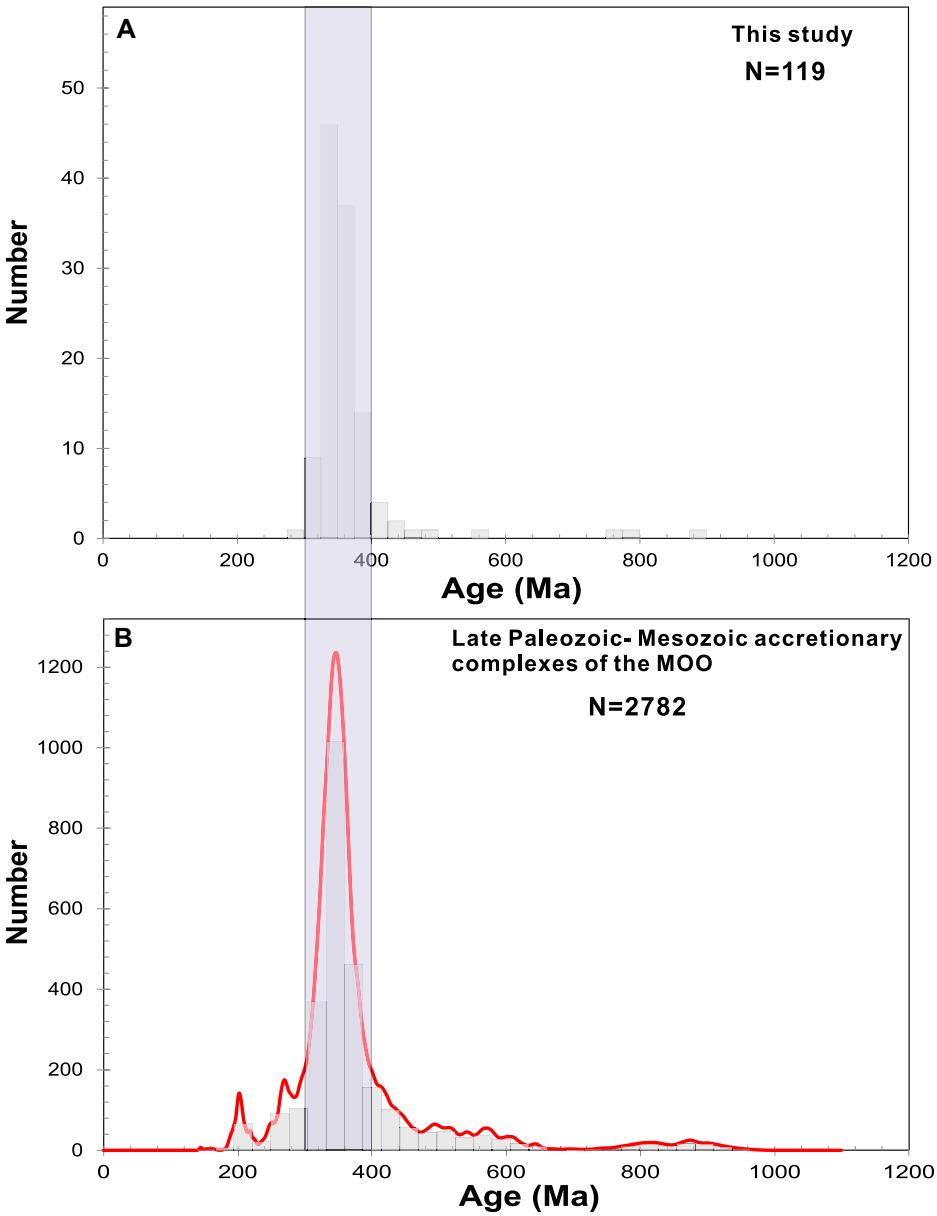

Figure 7. Comparison of detrital zircon populations of the shist from the Khoidgobi Formation of central Mongolia and the late Paleozoic–Mesozoic accretionary complexes of the Mongol-Okhotsk Ocean (MOO). Detrital zircon ages of the late Paleozoic–Mesozoic accretionary complexes (Table S4; see text footnote 1) are compiled from the literature of Kelty et al. (2008), Bussien et al. (2011), Hara et al. (2013), and Ruppen et al. (2014). N—number.

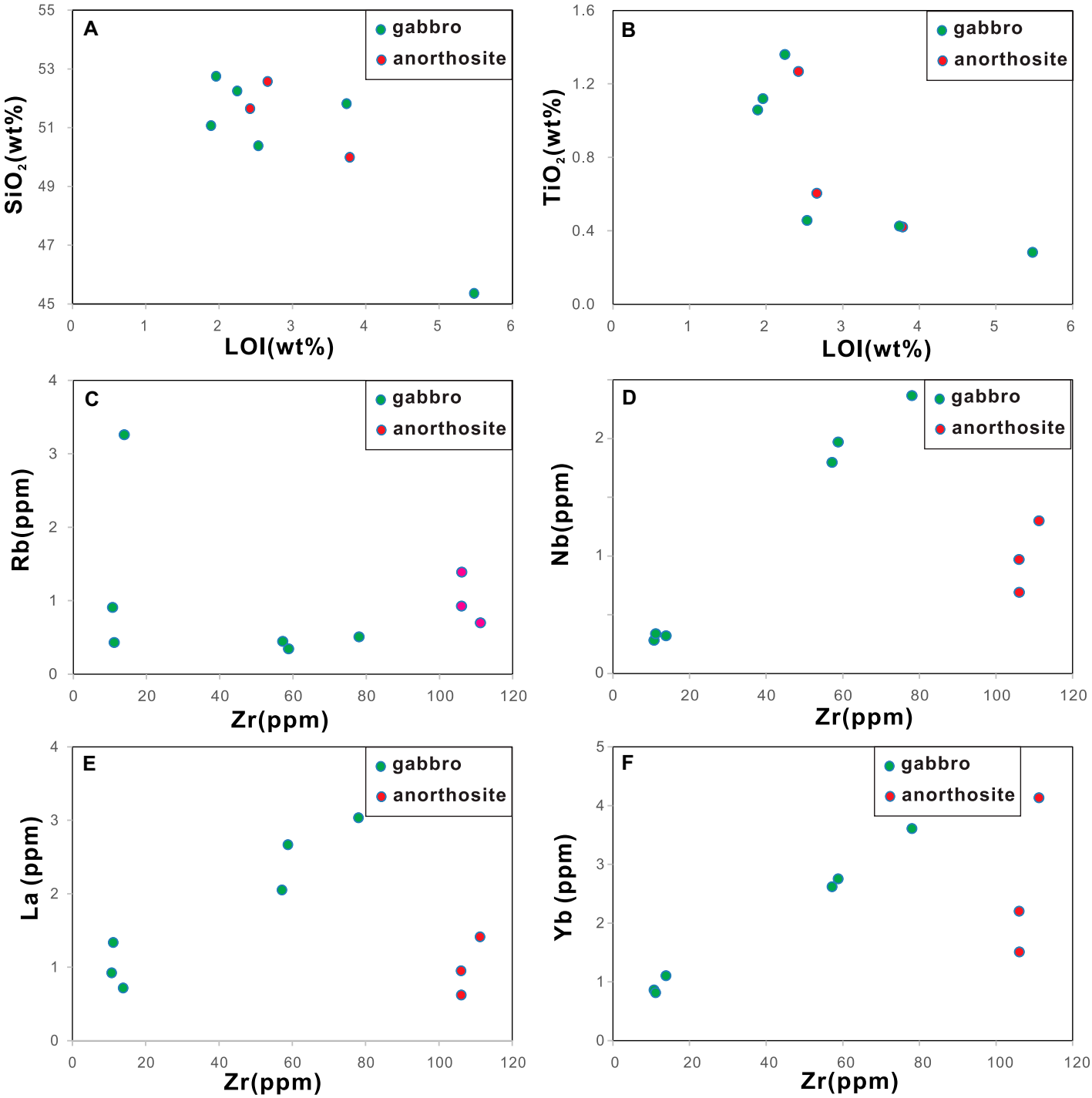

Figure 8. Plots of selected elements versus loss on ignition (LOI) or Zr to evaluate the mobility of elements in samples of the Erdendalai ophiolite from central Mongolia. (A) Plots of LOI versus SiO_2, (B) LOI versus TiO_2, (C) Zr versus Rb, (D) Zr versus Nb, (E) Zr versus La, and (F) Zr versus Yb.

Figure 9. Selected elements and their ratios plots for the gabbros of the Erdendalai ophiolite from central Mongolia. (A, B) Plots of SiO_2 versus Th/La and Nb/La to evaluate the crustal contamination. (C, D) Plots of Mg# versus Cr and Ni indicating fractional crystallization of olivine (Ol) and clinopyroxene (Cpx). (E, F) Plots of Cr versus Ni and Cr versus V implying Cpx crystallization (Rollinson, 1993). (G) Plots of SiO_2 versus Dy/Yb to exclude amphibole fractionation (Davidson et al., 2007). (H) Plots of TiO_2 versus MgO suggesting limited fractionation of Fe-Ti oxides. Hb—hornblende.

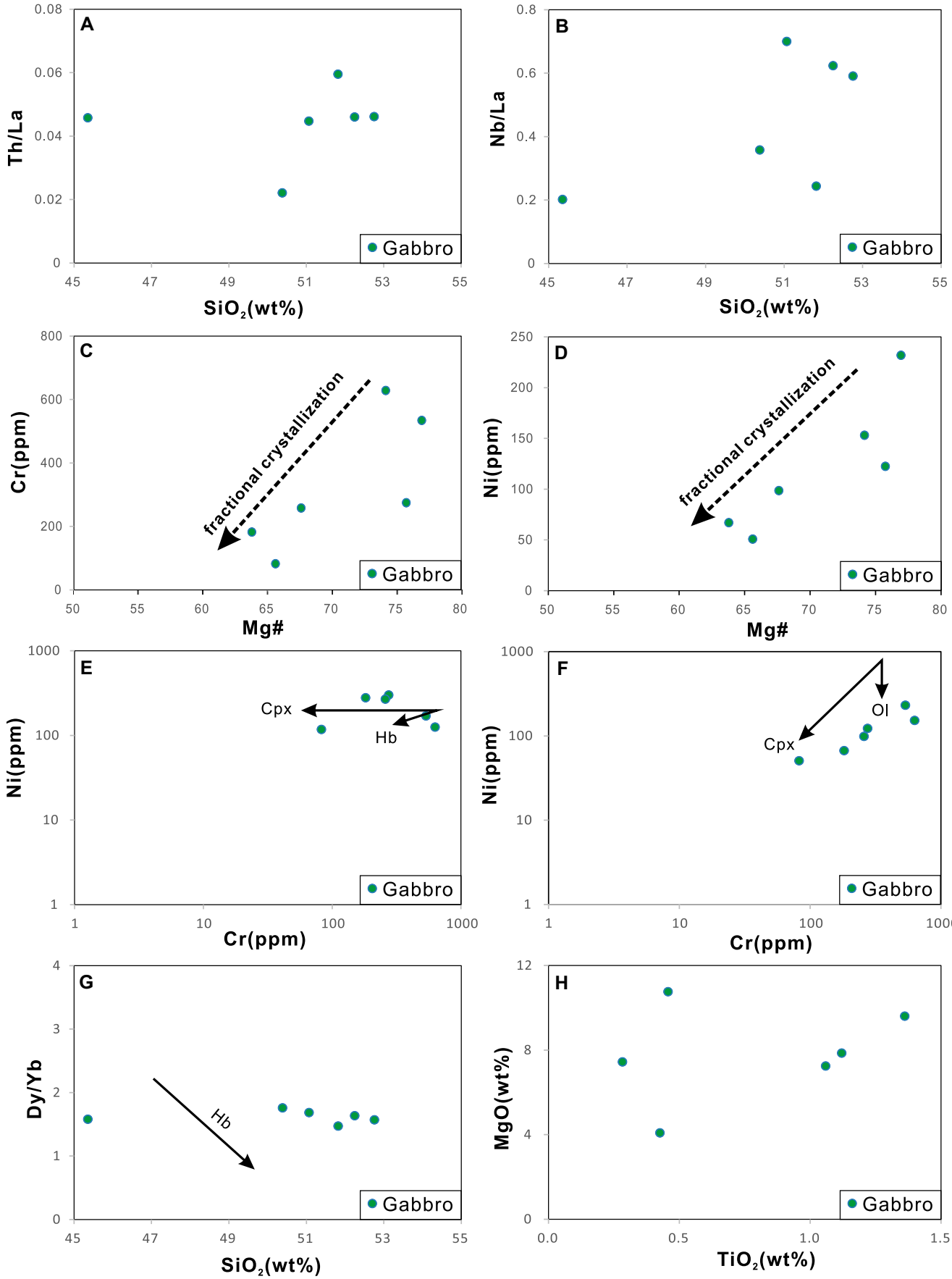

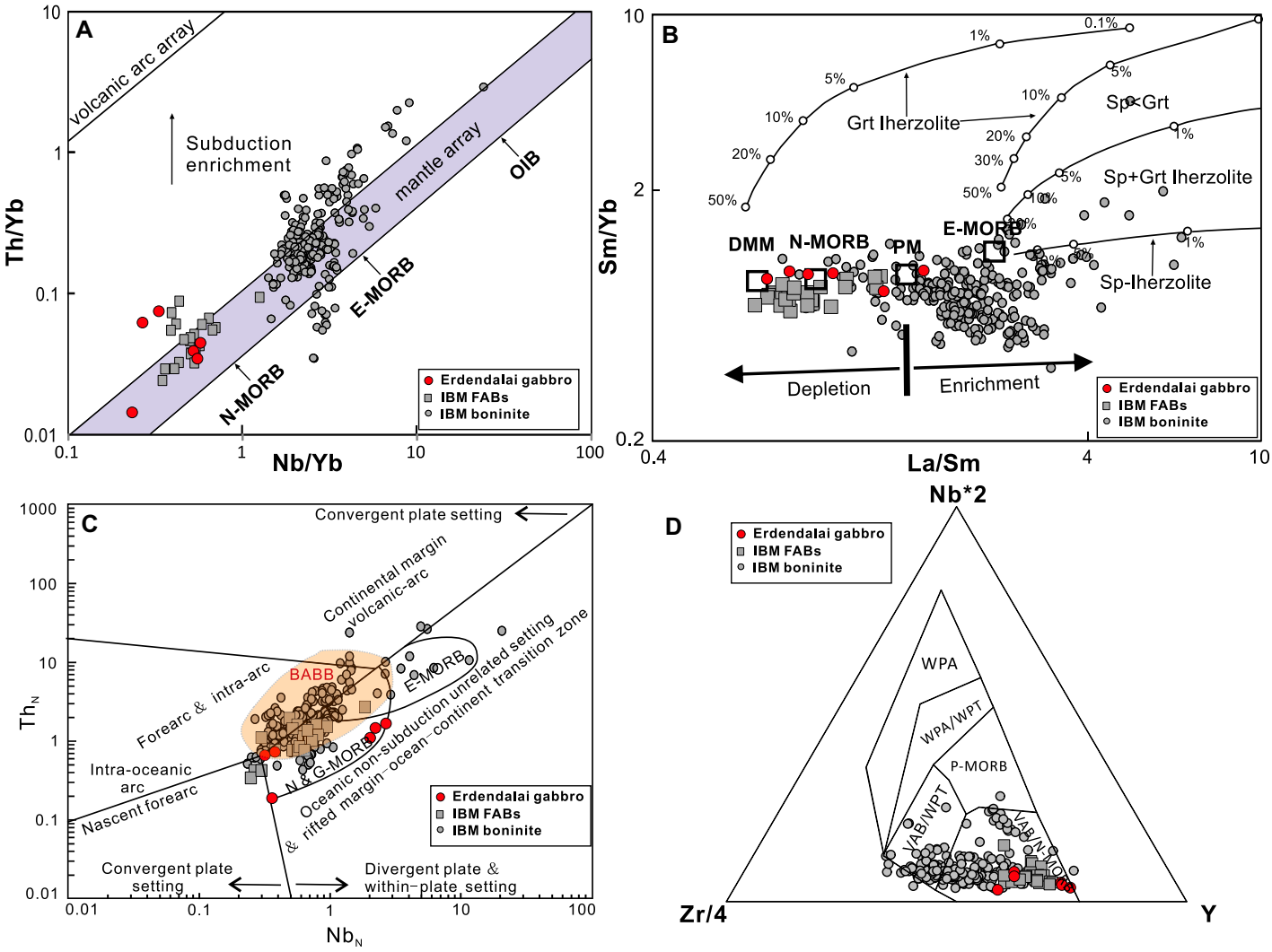

Figure 10. Geochemical plots of the gabbros from the Erdendalai ophiolite from central Mongolia. (A) Th/Yb versus Nb/Yb diagram (Pearce, 2008). (B) Sm/Yb versus La/Sm diagram (Aldanmaz et al., 2000). (C) Nb_N versus Th_N diagram (Saccani, 2015). (D) Nb-Zr-Y diagram (Meschede, 1986). Data sources of Izu–Bonin–Mariana (IBM) forearc basalts (FABs) are from Reagan et al. (2010) and data sources of IBM boninite are from Ishizuka et al. (2020) and Shervais et al. (2021). Normalizing values are from Sun and McDonough (1989). N-MORB—normal mid-ocean-ridge basalt; WPA—within-plate alkaline basalt; WPT—within-plate tholeiite; IAB—island-arc basalt; E-MORB—enriched mid-ocean-ridge basalt; P-MORB—plume-type mid-ocean-ridge basalt; PM—primitive mantle; DMM—depleted MORB mantle; OIB—ocean-island basalt; Grt—garnet; Sp—spinel; BABB—backarc basin basalt; VAB—volcanic-arc basalt; GMORB—garnet-influenced mid-oceanic-ridge basalt.

domain widely interpreted as having formed in a trench–accretionary wedge setting during the subduction of the MOO (Kurihara et al., 2009; Bussien et al., 2011). Tectonically, the Erdendalai ophiolite correlates with the Adaatsag and Khuhu Davaa ophiolites along the strike of the suture zone (Zhu et al., 2018, 2023a) but it is distinct from the backarc basin systems documented in the rear of the MOO's main magmatic arcs (Zhu et al., 2016, 2023c). Thus, the Carboniferous SSZ-type Erdendalai ophiolite, comprising identified FAB-like gabbro and boninite-derived anorthosite, provides key evidence for the presence of an intra-oceanic subduction-accretion system in the southwest MOO during the early Carboniferous.

6.3. Tectonic Evolution of the MOO

SSZ ophiolites are widely interpreted to preserve evidence of forearc extension in the upper plate during subduction initiation (Dilek and Furnes, 2011; Whattam and Stern, 2011). In particular, the volcanic crustal sequence of an SSZ ophiolite is expected to include earliest MORB-like FABs, overlain by boninites and other high-Mg andesites, and succeeded by arc tholeiites and calc-alkaline lithologies (Whattam and Stern, 2011; van Hinsbergen et al., 2015). Despite the common structural dismemberment and incomplete preservation of ophiolitic chemostratigraphy, the diagnostic presence of FABs and/or boninitic rocks within SSZ ophiolites is regarded as a key signature of the earliest volcanic activity linked to subduction initiation (Whattam and Stern, 2011; Stern et al., 2012; Hickey-Vargas et al., 2018). Our new findings provide important constraints on the subduction initiation history of the MOO.

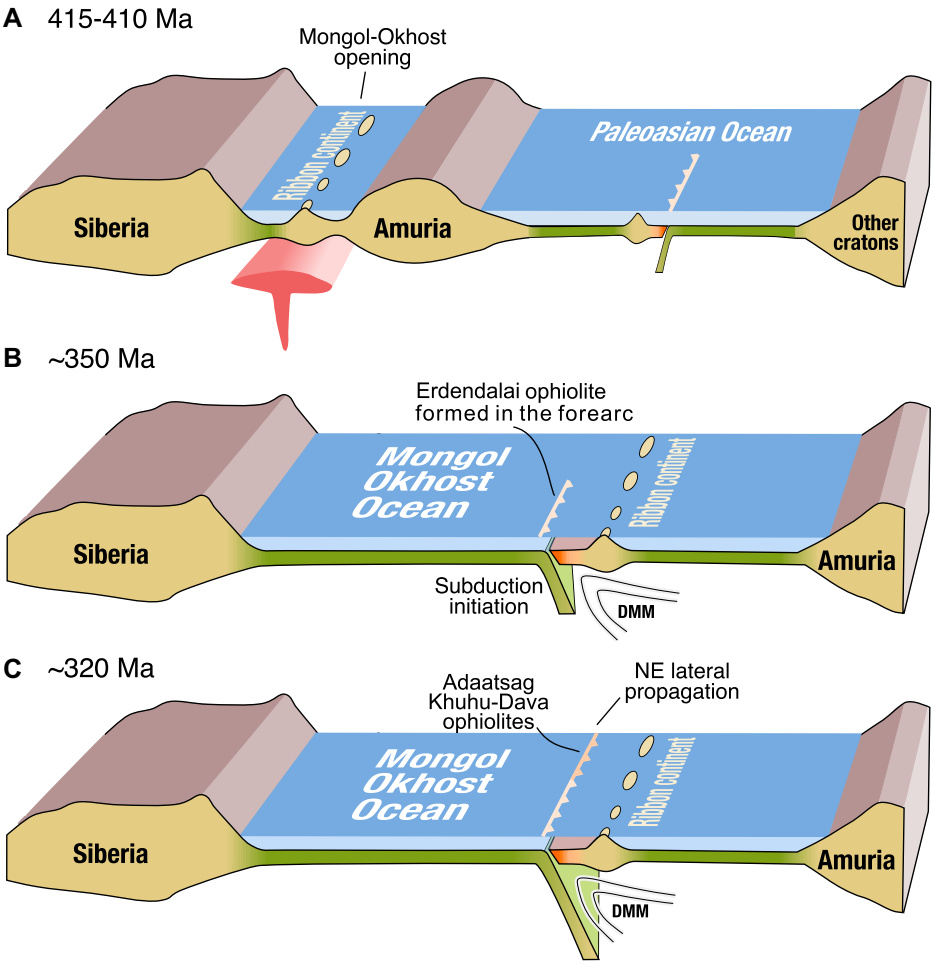

Figure 11. Schematic diagrams showing the proposed tectonic evolution of the Mongol-Okhotsk Ocean. DMM—depleted MORB mantle.

The gabbroic rocks from the Erdendalai ophiolite display only minor LILE enrichment relative to heavy REEs and HFSEs, along with slightly depleted Nb and Ta concentrations compared to N-MORB. These features indicate minimal contribution from slab-derived components. Collectively, the geochemical characteristics suggest that the gabbros are compositionally analogous to FABs, which are interpreted as the earliest magmatic products formed following subduction initiation (Reagan et al., 2010; Ishizuka et al., 2014; Hickey-Vargas et al., 2018). There are two end-member mechanisms of subduction initiation: spontaneous and induced (Stern, 2004; Stern and Gerya, 2018). Spontaneous subduction initiation is theorized to be triggered by gravitational instability, such as the negative buoyancy contrast across oceanic transform faults or passive continental margins, leading to lithospheric collapse without requiring external plate convergence (Stern, 2004; Arculus et al., 2015). In contrast, induced subduction initiation necessitates a period of forced plate convergence, which nucleates a new subduction zone along a pre-existing weak zone (Gurnis et al., 2004; Stern and Gerya, 2018). However, advanced numerical models demonstrate that even archetypal "spontaneous" settings require some degree of external horizontal forcing to initiate self-sustaining subduction (Zhong and Li, 2019; Liu et al., 2024). Given this modern understanding that favors a hybrid driving mechanism, and considering the Erdendalai ophiolite's formation within a pre-existing tectonic collage, we favor a model where the subduction initiation in the southwestern MOO was induced or at least critically facilitated by regional compressional stresses. These stresses could have been transmitted from distant plate boundaries or from the resistance to the opening of the MOO itself. Consequently, detailed structural analysis around the Erdendalai ophiolite remains a key objective for future work aimed at resolving its specific subduction initiation mechanism. In addition, the presence of ancient zircon grains within the Erdendalai ophiolite suggests inheritance from a continental crustal source. Although one might speculate that the collapse of a passive continental margin could initiate subduction and explain these signatures, both numerical models and geological evidence indicate that subduction initiation at passive margins is unlikely due to the high mechanical strength of lithosphere, which resists collapse—as exemplified by the stable Atlantic passive margin (e.g., Gurnis et al., 2004; Nikolaeva et al., 2011; Stern and Gerya, 2018). More critically, the depleted mantle signature and the absence of significant continental crustal contamination in the Erdendalai ophiolite argue against proximity to a thick continental margin during melt generation. Furthermore, as previously discussed, the geochemical characteristics of this SSZ ophiolite are consistent with formation in an intra-oceanic setting. We propose that the Erdendalai intra-oceanic arc was underlain, at least partially, by a continental fragment or relic that separated from the southern continental margin during the opening of the MOO. This model is supported by both modern and ancient analogues of oceanic arcs underlain by continental slivers (Tapster et al., 2014; Shao et al., 2015; Li et al., 2018). Numerical modeling further confirms that such microcontinental ribbons can play a critical role in localizing subduction nucleation (Zhu et al., 2023d). In the present case, we suggest that the presence of this continental sliver triggered, or at least facilitated, the initiation of southward subduction of the southwestern MOO plate—a mechanism comparable to that proposed for the Adaatsag-Khuhu Davaa intra-oceanic subduction system (Zhu et al., 2023a).

Based on integrated evidence from this study and previous works, we propose a revised tectonic model for the evolution of the MOO in the Mongolian segment (Fig. 11). The identification of Cambrian continental-type eclogites along with other high-grade metamorphic records indicates that microcontinental blocks and Neoproterozoic subduction-accretion complexes were accreted to the Siberian Craton during the early Paleozoic, likely associated with the closure of the Pan-Rodinian Mirovoi Ocean (e.g., Wilhem et al., 2012; Zhang et al., 2016; Buriánek et al., 2017; Zhou et al., 2018a; Yang et al., 2022; Zhu et al., 2023b). This interpretation is further supported by paleomagnetic data, which suggest that the microcontinents of the CAOB were in proximity to the Siberian Craton by the Early Cambrian (Kravchinsky et al., 2010). During the Early Devonian, a

mantle plume impinged upon and thermally eroded the lithosphere of the early Paleozoic accretionary collage, ultimately triggering rifting and the opening of the MOO. This model offers a coherent explanation for the observed crosscutting relationship wherein the younger Mongol-Okhotsk orogenic belt truncates the pre-existing early Paleozoic accretionary collage around the Siberian Craton (Zorin, 1999; Zhu et al., 2024b). During the opening of the MOO, one or several thin ribbon continents rifted away from its southern continental margin (Fig. 11A). These ribbon continents introduced critical lithospheric weaknesses and heterogeneities along the continent-ocean boundary, which facilitated the localization of new subduction zones during subsequent kinematic reorganization (Zhu et al., 2023d). By the early Mississippian, sinking of the oceanic lithosphere likely induced rapid trench rollback, enabling asthenospheric material to flow over the descending slab (Fig. 11B). This asthenospheric upwelling led to decompression melting (Stern and Gerya, 2018), generating MORB-like forearc basaltic gabbros and boninitic magmas (the parent magma of anorthosites; ca. 350 Ma) in the Erdendalai ophiolites. Similarly, in the northeastern segment of the MOO, subduction initiations occurred during the early Pennsylvanian, as evidenced by the Adaatsag and Khuhu Davaa SSZ ophiolites (Zhu et al., 2018, 2023a). The simplest scenario to explain the age difference is a subduction initiation in the southwest during the early Carboniferous, followed by lateral propagation toward the northeast (Fig. 11C). 3-D thermomechanical modeling suggest subduction initiation could laterally propagate along the transform away from the ridge, which can explain the systematic variations in ages of SSZ ophiolites in the Bitlis-Zagros suture zone (Zhou et al., 2018b). The propagation mechanism need not be limited to transform faults. As noted by Zhou et al. (2020), subduction can also jump to and advance along passive margins if significant lithospheric weaknesses exist and are leveraged by strong slab pull from a neighboring, established oceanic subduction zone. The subsequent change of the southern passive margin in central Mongolia to an active margin by the late Carboniferous, as evidenced by various magmatic records in the Middle Gobi belt (Zhu et al., 2023e), could be the direct consequence of this northeastward subduction zone propagating and eventually affecting the continental margin. However, with our current knowledge, we cannot rule out the possibility that these subduction zones initiated independently at different times. The observed age discrepancy between the Erdendalai ophiolite formation and the deposition of the Khoidgobi Formation clastic sediments can be explained by two tectonic models: (1) a progressive accretion and emplacement of the ophiolite and associated sediments within the forearc environment of an intraoceanic subduction zone. (2) Alternatively, the ophiolite was thrusted over a continental margin or microcontinent during a collisional event, with the accompanying sediments accumulating in a syn-collisional peripheral foreland basin. The detection of Precambrian and pre-Carboniferous zircon grains in the Khoidgobi Formation provides supporting evidence for the second, collision-related scenario.

7. CONCLUSIONS

The investigation of the Erdendalai ophiolite provides critical insights into the tectonic evolution of the southwestern Mongol-Okhotsk Orogenic Belt, with the following key conclusions:

(1) Zircon U-Pb dating of anorthosite yields a crystallization age of ca. 350 Ma for the Erdendalai ophiolite, indicating the presence of a mature Mongol-Okhotsk Ocean capable of generating oceanic crust by the early Carboniferous. The discovery of the Erdendalai ophiolite provides the first robust ophiolitic evidence to trace the southwestern extension of the Mongol-Okhotsk suture zone in Mongolia.

(2) The geochemical signatures of the gabbros (forearc basalt–like) and anorthosites (derived from boninitic precursors) are diagnostic of formation in an intra-oceanic forearc setting, indicating subduction of the southwestern Mongol-Okhotsk Ocean had already initiated by the early Carboniferous. The age variations of Carboniferous supra-subduction zone ophiolites may reflect lateral propagation of the subduction initiation. The depositional age (post–ca. 302 Ma) of the enclosing Khoidgobi Formation accretionary complex sediments indicates that the obduction and accretion of this oceanic lithosphere onto the continental margin occurred during the latest Carboniferous or later.

ACKNOWLEDGMENTS

We are grateful to Chun Yang, Mingzhu Ma, Liqin Zhou, Xiaochao Che, Chenghao Liu, and Shuangrong Zhang for their support of the analytical experiments. This work was financially supported by the Xinjiang Uygur Autonomous Region Key Research and Development Project (2024B03006-2) and the National Natural Science Foundation of China (grant 42272262). DPG is funded by grant PID2021-128801NA-I00 funded by MCIN/AEI/10.13039/501100011033. This study is also a contribution to the Theory of Hydrocarbon Enrichment under Multi-Spheric Interactions of the Earth project, Institute of Geology and Geophysics, Chinese Academy of Sciences.

REFERENCES CITED

Aigner-Torres, M., Blundy, J., Ulmer, P., and Pettke, T., 2007, Laser Ablation ICPMS study of trace element partitioning between plagioclase and basaltic melts: An experimental approach: Contributions to Mineralogy and Petrology, v. 153, p. 647–667, https://doi.org/10.1007/s00410-006-0168-2.

Aldanmaz, E., Pearce, J.A., Thirwall, M.F., and Mitchell, J.G., 2000, Petrogenetic evolution of late Cenozoic post-collision volcanism in western Anatolia, Turkey: Journal of Volcanology and Geothermal Research, v. 102, p. 67–95, https://doi.org/10.1016/S0377-0273(00)00182-7.

Arculus, R.J., et al., 2015, A record of spontaneous subduction initiation in the Izu–Bonin–Mariana Arc: Nature Geoscience, v. 8, p. 728–733, https://doi.org/10.1038/ngeo2515.

Badarch, G., Cunningham, W.D., and Windley, B.F., 2002, A new terrane subdivision for Mongolia: Implications for the Phanerozoic crustal growth of Central Asia: Journal of Asian Earth Sciences, v. 21, p. 87–110, https://doi.org/10.1016/S1367-9120(02)00017-2.

Bold, M., Tsujimori, T., Pastor-Galán, D., Adachi, T., Nakano, N., and Osanai, Y., 2025, Tectono-magmatic evolution of the Mongolian Collage with new evidence from the Ereendavaa Block: Gondwana Research, v. 147, p. 276–300, https://doi.org/10.1016/j.gr.2025.06.023.

Buriánek, D., Schulmann, K., Hrdličkova, K., Hanžl, P., Janoušek, V., Gerdes, A., and Lexa, O., 2017, Geochemical and geochronological constraints on distinct Early-Neoproterozoic and Cambrian accretionary events along southern margin of the Baydrag Continent in western Mongolia: Gondwana Research, v. 47, p. 200–227, https://doi.org/10.1016/j.gr.2016.09.008.

Bussien, D., Gombojav, N., Winkler, W., and Quadt, A., 2011, The Mongol–Okhotsk Belt in Mongolia—An appraisal of the geodynamic development by the study of sandstone provenance and detrital zircons: Tectonophysics, v. 510, p. 132–150, https://doi.org/10.1016/j.tecto.2011.06.024.

Compston, W., Williams, I.S., and Mayer, C., 1984, U-Pb geochronology of zircons from Lunar Breccia 73217 using a Sensitive High Resolution Ion Microprobe: Proceedings of the XIV Lunar Planetary Science Conference: Journal of Geophysical Research: Solid Earth, v. 89, no. S02, p. B525–B534, https://doi.org/10.1029/JB089iS02p0B525.

Crawford, A.J., 1989, Boninites and Related Rocks: London, Unwin Hyman, 496 p.

Davidson, J., Turner, S., Handley, H., MacPherson, C., and Dosseto, A., 2007, Amphibole "sponge" in arc crust?: Geology, v. 35, p. 787–790, https://doi.org/10.1130/G23637A.1.

Dilek, Y., and Furnes, H., 2009, Structure and geochemistry of Tethyan ophiolites and their petrogenesis in subduction rollback systems: Lithos, v. 113, p. 1–20, https://doi.org/10.1016/j.lithos.2009.04.022.

Dilek, Y., and Furnes, H., 2011, Ophiolite genesis and global tectonics: Geochemical and tectonic fingerprinting of ancient oceanic lithosphere: Geological Society of America Bulletin, v. 123, p. 387–411, https://doi.org/10.1130/B30446.1.

Domeier, M., 2018, Early Paleozoic tectonics of Asia: Towards a full-plate model: Geoscience Frontiers, v. 9, no. 3, p. 789–862, https://doi.org/10.1016/j.gsf.2017.11.012.

Donskaya, T.V., Gladkochub, D.P., Mazukabzov, A.M., and Ivanov, A.V., 2013, Late Paleozoic–Mesozoic subduction-related magmatism at the southern margin of the Siberian continent and the 150 million-year history of the Mongol–Okhotsk Ocean: Journal of Asian Earth Sciences, v. 62, p. 79–97, https://doi.org/10.1016/j.jseaes.2012.07.023.

Drake, M.J., and Weill, D.F., 1975, Partition of Sr, Ba, Ca, Y, Eu^{2+}, Eu^{3+}, and other REE between plagioclase feldspar and magmatic liquid: An experimental study: Geochimica et Cosmochimica Acta, v. 39, p. 689–712, https://doi.org/10.1016/0016-7037(75)90011-3.

Erdenechimeg, D., and Enkhabayar, B., 2017, Report on the results of geological mapping in Mongolia at 1:500,000 scale: Ulaanbaatar, Mongolia, National Geological Survey of Mongolia, report 8480 [in Mongolian].

Frey, F.A., Green, D.H., and Roy, S.D., 1978, Integrated models of basalt petrogenesis: A study of quartz tholeiites to olivine melilitites from South Eastern Australia utilizing geochemical and experimental petrological data: Journal of Petrology, v. 19, p. 463–513, https://doi.org/10.1093/petrology/19.3.463.

Ganbat, A., Tsujimori, T., Miao, L.C., Safonova, I., Pastor-Gal′an, D., Anaad, C., Baatar, M., Aoki, S., Aoki, K., and Savinskiy, I., 2021, Late Paleozoic-Early Mesozoic granitoids in the Khangay-Khentey basin, Central Mongolia: Implication for the tectonic evolution of the Mongol-Okhotsk Ocean margin: Lithos, v. 404–405, https://doi.org/10.1016/j.lithos.2021.106455.

Gladkochub, D.P., Donskaya, T.V., Wingate, M.T.D., Poller, U., Kroner, A., Fedorovsky, V.S., Mazukabov, A.M., Todt, W., and Pisarevsky, S.A., 2008, Petrology, geochronology, and tectonic implications of c. 500 Ma metamorphic and igneous rocks along the northern margin of the Central Asian Orogen (Olkhon terrane, Lake Baikal, Siberia): Journal of the Geological Society, v. 165, p. 235–246, https://doi.org/10.1144/0016-76492006-125.

Golowin, R., Portnyagin, M., Hoernle, K., Sobolev, A., Kuzmin, D., and Werner, R., 2017, The role and conditions of second-stage mantle melting in the generation of low-Ti tholeiites and boninites: The case of the Manihiki Plateau and the Troodos ophiolite: Contributions to Mineralogy and Petrology, v. 172, no. 11–12, https://doi.org/10.1007/s00410-017-1424-3.

Guilmette, C., Smit, M.A., van Hinsbergen, D.J.J., Corfu, F., Gürer, D., Charette, B., Maffione, M., Rabeau, O., and Savard, D., 2018, Forced subduction initiation revealed by crust-sole geochronology of the Semail ophiolite: Nature Geoscience, v. 11, p. 688–695, https://doi.org/10.1038/s41561-018-0209-2.

Gurnis, M., Hall, C., and Lavier, L., 2004, Evolving force balance during incipient subduction: Geochemistry, Geophysics, Geosystems, v. 5, https://doi.org/10.1029/2003GC000681.

Hara, H., Kurihara, T., Tsukada, K., Kon, Y., Uchino, T., Suzuki, T., Takeuchi, M., Nakane, Y., Nuramkhaan, M., and Chuluun, M., 2013, Provenance and origins of a Late Paleozoic accretionary complex within the Khangai–Khentei belt in the Central Asian Orogenic Belt, central Mongolia: Journal of Asian Earth Sciences, v. 75, p. 141–157, https://doi.org/10.1016/j.jseaes.2013.07.019.

Hickey-Vargas, R., Yogodzinski, G.M., Bizimis, M., Ishizuka, O., McCarthy, A., Kusano, Y., Savov, I.P., and Arculus, R., 2018, Origin of depleted basalts during subduction initiation: Evidence from IODP Expedition 351 Site U1438, Amami Sankaku Basin: Geochimica et Cosmochimica Acta, v. 229, p. 85–111, https://doi.org/10.1016/j.gca.2018.03.007.

Ishizuka, O., Tani, K., Reagan, M.K., Kanayama, K., Umino, S., Harigane, Y., Sakamoto, I., Miyajima, Y., Yuasa, M., and Dunkley, D.J., 2011, The time scales of subduction initiation and subsequent evolution of an oceanic island arc: Earth and Planetary Science Letters, v. 306, p. 229–240, https://doi.org/10.1016/j.epsl.2011.04.006.

Ishizuka, O., Tani, K., and Reagan, M.K., 2014, Izu–Bonin–Mariana forearc crust as a modern ophiolite analogue: Elements, v. 10, no. 2, p. 115–120, https://doi.org/10.2113/gselements.10.2.115.

Ishizuka, O., Taylor, R.N., Umino, S., and Kanayama, K., 2020, Geochemical evolution of arc and slab following subduction initiation: A record from the Bonin Islands, Japan: Journal of Petrology, v. 61, https://doi.org/10.1093/petrology/egaa050.

Jackson, S.E., Pearson, N.J., Griffin, W.L., and Belousova, E.A., 2004, The application of laser ablation-inductively coupled plasma-mass spectrometry to in situ U-Pb zircon geochronology: Chemical Geology, v. 211, p. 47–69, https://doi.org/10.1016/j.chemgeo.2004.06.017.

Jahn, B.M., Wu, F.Y., and Chen, B., 2000, Granitoids of the Central Asian orogenic belt and continental growth in the Phanerozoic: Earth and Environmental Science Transactions of the Royal Society of Edinburgh, v. 91, no. 1–2, p. 181–193, https://doi.org/10.1017/S0263593300007367.

Jahn, B.M., Windley, B., Natal'in, B., and Dobretsov, N., 2004, Phanerozoic continental growth in Central Asia: Journal of Asian Earth Sciences, v. 23, p. 599–603, https://doi.org/10.1016/S1367-9120(03)00124-X.

Jamyandorj, U., Tungalag, F., and Boishenko, A.F., 1990, Geological map of the Central and Eastern Mongolia, scale 1:500,000: Ulaanbaatar, Mongolia, Institute of Geological Research, Regional Geological Sector, Ministry of Heavy Industry [in Mongolian].

Jian, P., Kroner, A., and Zhou, G.Z., 2012, SHRIMP zircon U-Pb ages and REE partition for high-grade metamorphic rocks in the north Dabie complex: Insight into crustal evolution with respect to Triassic UHP metamorphism in east-central China: Chemical Geology, v. 328, p. 49–69, https://doi.org/10.1016/j.chemgeo.2012.01.015.

Kelty, T.K., Yin, A., Dash, B., Gehrels, G.E., and Ribeiro, A.E., 2008, Detrital-zircon geochronology of Paleozoic sedimentary rocks in the Hangay–Hentey basin, north-central Mongolia: Implications for the tectonic evolution of the Mongol–Okhotsk Ocean in central Asia: Tectonophysics, v. 451, p. 290–311, https://doi.org/10.1016/j.tecto.2007.11.052.

Kravchinsky, V.A., Sklyarov, E.V., Gladkochub, D.B., and Harbert, W.P., 2010, Paleomagnetism of the Precambrian Eastern Sayan rocks: Implications for the Ediacaran–Early Cambrian paleogeography of the Tuva–Mongolian composite terrane: Tectonophysics, v. 486, no. 1–4, p. 65–80, https://doi.org/10.1016/j.tecto.2010.02.010.

Kurihara, T., Tsukada, K., Otoh, S., Kashiwagi, K., Minjin, C.h., Dorjsuren, B., Bujinlkham, B., Sersmaa, G., Manchuk, N., Niwa, M., Tokiwa, T., Hikichi, G., and Kozuka, T., 2009, Upper Silurian and Devonian pelagic deep-water radiolarian chert from the Khangai-Khentei belt of Central Mongolia: Evidence for Middle Paleozoic subduction-accretion in the Central Asian Orogenic Belt: Journal of Asian Earth Sciences, v. 34, p. 209–225, https://doi.org/10.1016/j.jseaes.2008.04.010.

Li, T.D., Daukeev, S.Z., Kim, B.C., Tomurtogoo, O., and Petrov, O.V., 2008, Atlas of Geological Maps of Central Asia and Adjacent Areas: Beijing, Geological Publishing House.

Li, X.H., Abd El-Rahman, Y., Abu Anbar, M., Li, J., Ling, X.X., Wu, L.G., and Masoud, A.E., 2018, Old continental crust underlying juvenile oceanic arc: Evidence from northern Arabian-Nubian Shield, Egypt: Geophysical Research Letters, v. 45, p. 3001–3008, https://doi.org/10.1002/2018GL077121.

Liu, H., Li, Y., He, H., Huangfu, P., and Liu, Y., 2018, Two-phase southward subduction of the Mongol-Okhotsk oceanic plate constrained by Permian-Jurassic granitoids in the Erguna and Xing'an massifs (NE China): Lithos, v. 304–307, p. 347–361, https://doi.org/10.1016/j.lithos.2018.01.016.

Liu, L., Li, H.-Y., Liu, L.-j., Ryan, J.G., Morgan, J.P., Ren, K.-X., and Xu, Y.-G., 2024, Horizontally forced initiation of the Izu-Bonin-Mariana subduction zone: Communications Earth & Environment, v. 5, https://doi.org/10.1038/s43247-024-01263-4.

Ludwig, K.R., 2001, Squid 1.03 A User's Manual: Berkeley, California, Berkeley Geochronology Center Special Publication 2, 19 p.

Ludwig, K.R., 2003, User's Manual for Isoplot 3.00: A Geochronological Toolkit for Microsoft Excel: Berkeley, California, Berkeley Geochronology Center Special Publication 4, 70 p.

Meschede, M., 1986, A method of discriminating between different types of mid-ocean ridge basalts and continental tholeiites with the Nb-Zr-Y diagram: Chemical Geology, v. 56, no. 3–4, p. 207–218, https://doi.org/10.1016/0009-2541(86)90004-5.

Miao, L.C., Baatar, M., Zhang, F.Q., Anaad, C., Zhu, M.S., and Yang, S.H., 2016, Cambrian Kherlen ophiolite in northeastern Mongolia and its tectonic implications: SHRIMP zircon dating and geochemical constraints: Lithos, v. 261, p. 128–143, https://doi.org/10.1016/j.lithos.2015.12.012.

Miao, L.C., Zhang, F.Q., Baatar, M., Zhu, M.S., and Anaad, C., 2017, SHRIMP zircon U-Pb ages and tectonic implications of igneous events in the Ereendavaa metamorphic terrane in NE Mongolia: Journal of Asian Earth Sciences, v. 144, p. 243–260, https://doi.org/10.1016/j.jseaes.2017.03.005.

Nakamura, K., Kato, Y., Tamaki, K., and Ishii, T., 2007, Geochemistry of hydrothermally altered basaltic rocks from the Southwest Indian Ridge near the Rodriguez Triple Junction: Marine Geology, v. 239, p. 125–141, https://doi.org/10.1016/j.margeo.2007.01.003.

Narantsetseg, T., Orolmaa, D., Yuan, C., Wang, T., Guo, L., Tong, Y., Wang, X., Orshikh, O.E., Oyunchimeg, T., Delgerzaya, P., and Enkhdalai, B., 2019, Early-middle Paleozoic volcanic rocks from the Ereendavaa terrane (Tsarigiin gol area, NE Mongolia) with implications for tectonic evolution of the Kherlen massif: Journal of Asian Earth Sciences, v. 175, p. 138–157, https://doi.org/10.1016/j.jseaes.2018.12.008.

Nikolaeva, K., Gerya, T.V., and Marques, F.O., 2011, Numerical analysis of subduction initiation risk along the Atlantic American passive margins: Geology, v. 39, p. 463–466, https://doi.org/10.1130/G31972.1.

Parfenov, L.M., Popeko, L.I., and Tomurtogoo, O., 2001, Problems of tectonics of the Mongol–Okhotsk orogenic belt: Geology of the Pacific Ocean, v. 16, p. 797–830.

Paton, C., Woodhead, J.D., Hellstrom, J.C., Hergt, J.M., Greig, A., and Maas, R., 2010, Improved laser ablation U-Pb zircon geochronology through robust downhole fractionation correction: Geochemistry, Geophysics, Geosystems, v. 11, https://doi.org/10.1029/2009GC002618.

Pearce, J.A., 2003, Supra-subduction zone ophiolites: The search for modern analogues, *in* Dilek, Y., and Newcomb, S., eds., Ophiolite Concept and the Evolution of Geological Thought: Geological Society of America Special Paper 373, p. 269–293, https://doi.org/10.1130/0-8137-2373-6.269.

Pearce, J.A., 2008, Geochemical fingerprinting of oceanic basalts with applications to ophiolite classification and the search for Archean oceanic crust: Lithos, v. 100, no. 1–4, p. 14–48, https://doi.org/10.1016/j.lithos.2007.06.016.

Pearce, J.A., 2014, Immobile element fingerprinting of ophiolites: Elements, v. 10, p. 101–108, https://doi.org/10.2113/gselements.10.2.101.

Piccardo, G.B., and Guarnieri, L., 2011, Gabbro-norite cumulates from strongly depleted MORB melts in the Alpine–Apennine ophiolites: Lithos, v. 124, no. 3–4, p. 200–214, https://doi.org/10.1016/j.lithos.2011.01.017.

Pilot, J., Werner, C.D., Haubrich, F., and Baumann, N., 1998, Palaeozoic and Proterozoic zircons from the mid-Atlantic ridge: Nature, v. 393, p. 676–679, https://doi.org/10.1038/31452.

Pirajno, F., Mao, J.W., Zhang, Z.C., Zhang, Z.H., and Chai, F.M., 2008, The association of mafic-ultramafic intrusions and A-type magmatism in the Tian Shan and Altay orogens, NW China: Implications for geodynamic evolution and potential for the discovery of new ore deposits: Journal of Asian Earth Sciences, v. 32, p. 165–183, https://doi.org/10.1016/j.jseaes.2007.10.012.

Reagan, M.K., Ishizuka, O., Stern, R.J., Kelley, K.A., Ohara, Y., Blichert-Toft, J., Bloomer, S.H., Cash, J., Fryer, P., Hanan, B., Hickey-Vargas, R., Ishii, T., Kimura, J.-I., Peate, D.W., Rowe, M.C., and Woods, M., 2010, Fore-arc basalts and subduction initiation in the Izu–Bonin–Mariana system: Geochemistry, Geophysics, Geosystems, v. 11, p. 1–17, https://doi.org/10.1029/2009GC002871.

Rollinson, H.R., 1993, Using Geochemical Data: Evaluation, Presentation, Interpretation: London, Longman, 352 p.

Ross, P.S., and Bédard, J.H., 2009, Magmatic affinity of modern and ancient subalkaline volcanic rocks determined from trace-element discriminant diagrams: Canadian Journal of Earth Sciences, v. 46, no. 11, p. 823–839, https://doi.org/10.1139/E09-054.

Rubatto, D., 2002, Zircon trace element geochemistry: Partitioning with garnet and the link between U-Pb ages and metamorphism: Chemical Geology, v. 184,

no. 1–2, p. 123–138, https://doi.org/10.1016/S0009-2541(01)00355-2.

Ruppen, D., Knaf, A., Bussien, D., Winkler, W., Chmedtseren, A., and von Quadt, A., 2014, Restoring the Silurian to Carboniferous northern active continental margin of the Mongol–Okhotsk Ocean in Mongolia: Hangay–Hentey accretionary wedge and seamount collision: Gondwana Research, v. 25, no. 4, p. 1517–1534.

Saccani, E., 2015, A new method of discriminating different types of post-Archean ophiolitic basalts and their tectonic significance using Th-Nb and Ce-Dy-Yb systematics: Geoscience Frontiers, v. 6, p. 481–501, https://doi.org/10.1016/j.gsf.2014.03.006.

Schulmann, K., and Paterson, S., 2011, Asian continental growth: Nature Geoscience, v. 4, p. 827–829, https://doi.org/10.1038/ngeo1339.

Şengör, A.M.C., Natal'in, B.A., and Burtman, U.S., 1993, Evolution of the Altaid tectonic collage and Paleozoic crustal growth in Eurasia: Nature, v. 364, p. 299–307, https://doi.org/10.1038/364299a0.

Shao, W.Y., Chung, S.L., Chen, W.S., Lee, H.Y., and Xie, L.W., 2015, Old continental zircons from a young oceanic arc, eastern Taiwan: Implications for Luzon subduction initiation and Asian accretionary orogeny: Geology, v. 43, p. 479–482, https://doi.org/10.1130/G36499.1.

Shervais, J.W., et al., 2021, Magmatic response to subduction initiation, Part II: Boninites and related rocks of the Izu-Bonin Arc from IOPD Expedition 352: Geochemistry, Geophysics, Geosystems, v. 22, https://doi.org/10.1029/2020GC009093.

Sláma, J., Košler, J., Condon, D.J., Crowley, J.L., Gerdes, A., Hanchar, J.M., Horstwood, M.S.A., Morris, G.A., Nasdala, L., Norberg, N., and Schaltegger, U., 2008, Plešovice zircon—A new natural reference material for U-Pb and Hf isotopic microanalysis: Chemical Geology, v. 249, p. 1–35, https://doi.org/10.1016/j.chemgeo.2007.11.005.

Sorokin, A.A., Zaika, V.A., Kovach, V.P., Kotov, A.B., Xu, W., and Yang, H., 2020, Timing of closure of the eastern Mongol–Okhotsk Ocean: Constraints from U-Pb and Hf isotopic data of detrital zircons from metasediments along the Dzhagdy Transect: Gondwana Research, v. 81, p. 58–78, https://doi.org/10.1016/j.gr.2019.11.009.

Sotiriou, P., and Polat, A., 2020, Comparisons between Tethyan anorthosite-bearing ophiolites and Archean anorthosite-bearing layered intrusions: Implications for Archean geodynamic processes: Tectonics, v. 39, no. 8, https://doi.org/10.1029/2020TC006096.

Sotiriou, P., and Polat, A., 2023, Petrogenesis of anorthosites throughout Earth history: Precambrian Research, v. 384, https://doi.org/10.1016/j.precamres.2022.106936.

Stern, R.J., 2002, Subduction zones: Reviews of Geophysics, v. 40, no. 4, p. 1012.

Stern, R.J., 2004, Subduction initiation: Spontaneous and induced: Earth and Planetary Science Letters, v. 226, p. 275–292, https://doi.org/10.1016/S0012-821X(04)00498-4.

Stern, R.J., and Gerya, T., 2018, Subduction initiation in nature and models: A review: Tectonophysics, v. 746, p. 173–198, https://doi.org/10.1016/j.tecto.2017.10.014.

Stern, R.J., Reagan, M., Ishizuka, O., Ohara, Y., and Whattam, S., 2012, To understand subduction initiation, study forearc crust: To understand forearc crust, study ophiolites: Lithosphere, v. 4, p. 469–483, https://doi.org/10.1130/L183.1.

Sun, S.-s., and McDonough, W.F., 1989, Chemical and isotopic systematics of oceanic basalts: Implications for mantle composition and processes, *in* Saunders, A.D., and Norry, M.J., eds., Magmatism in the Ocean Basins: Geological Society, London, Special Publication 42, p. 313–345, https://doi.org/10.1144/GSL.SP.1989.042.01.19.

Takagi, D., Sato, H., and Nakagawa, M., 2005, Experimental study of a low-alkali tholeiite at 1–5 kbar: Optimal condition for the crystallization of high-An plagioclase in hydrous arc tholeiite: Contributions to Mineralogy and Petrology, v. 149, no. 5, p. 527–540, https://doi.org/10.1007/s00410-005-0666-7.

Tang, J., Xu, W.L., Wang, F., Zhao, S., and Wang, W., 2016, Early Mesozoic southward subduction history of the Mongol–Okhotsk oceanic plate: Evidence from geochronology and geochemistry of early Mesozoic intrusive rocks in the Erguna Massif: Gondwana Research, v. 31, p. 218–240, https://doi.org/10.1016/j.gr.2014.12.010.

Tapster, S., Roberts, N.M.W., Petterson, M.G., Saunders, A.D., and Naden, J., 2014, From continent to intra-oceanic arc: Zircon xenocrysts record the crustal evolution of the Solomon island arc: Geology, v. 42, p. 1087–1090, https://doi.org/10.1130/G36033.1.

Tomurtogoo, O., Windley, B.F., Kroner, A., Badarch, G., and Liu, D.Y., 2005, Zircon age and occurrence of the Adaatsag ophiolite and Muron shear zone, central Mongolia: Constraints on the evolution of the Mongol–Okhotsk ocean, suture and orogen: Journal of the Geological Society, v. 162, p. 125–134, https://doi.org/10.1144/0016-764903-146.

Van der Voo, R., van Hinsbergen, D.J., Domeier, M., Spakman, W., and Torsvik, T.H., 2015, Latest Jurassic–earliest Cretaceous closure of the Mongol–Okhotsk Ocean: A paleomagnetic and seismological-tomographic analysis, *in* Van der Voo, R., van Hinsbergen, D.J.J., Domeier, M., Spakman, W., and Torsvik, T.H., eds., Late Jurassic Margin of Laurasia—A Record of Faulting Accommodating Plate Rotation: Geological Society of America Special Paper 513, p. 589–606, https://doi.org/10.1130/2015.2513(19).

van Hinsbergen, D.J.J., et al., 2015, Dynamics of intraoceanic subduction initiation: 2. Suprasubduction zone ophiolite formation and metamorphic sole exhumation in context of absolute plate motions: Geochemistry, Geophysics, Geosystems, v. 16, p. 1771–1785, https://doi.org/10.1002/2015GC005745.

Wang, T., Tong, Y., Xiao, W.J., Guo, L., Windley, B.F., Donskaya, T., Li, S., Narantsetseg, T., and Zhang, J.J., 2022, Rollback, scissor-like closure of the Mongol-Okhotsk Ocean and formation of an orocline: Magmatic migration based on a large archive of age-data: National Science Review, v. 9, https://doi.org/10.1093/nsr/nwab210.

Wang, T., Xiao, W., Collins, W.J., Tong, Y., Hou, Z., Huang, H., Wang, X., Lin, S., Seltmann, R., Wang, C., and Han, B., 2023, Quantitative characterization of orogens through isotopic mapping: Communications Earth & Environment, v. 4, https://doi.org/10.1038/s43247-023-00779-5.

Whattam, S.A., and Stern, R.J., 2011, The 'subduction initiation rule': A key for linking ophiolites, intra-oceanic forearcs, and subduction initiation: Contributions to Mineralogy and Petrology, v. 162, no. 5, p. 1031–1045, https://doi.org/10.1007/s00410-011-0638-z.

Wilhem, C., Windley, B.F., and Stampfli, G.M., 2012, The Altaids of Central Asia: A tectonic and evolutionary innovative review: Earth-Science Reviews, v. 113, no. 3–4, p. 303–341, https://doi.org/10.1016/j.earscirev.2012.04.001.

Wilson, M., ed., 1989, Igneous Petrogenesis: A Global Tectonic Approach: London, Unwin Hyman, 466 p., https://doi.org/10.1007/978-1-4020-6788-4.

Windley, B.F., Alexeiev, D., Xiao, W., Kroner, A., and Badarch, G., 2007, Tectonic models for accretion of the Central Asian Orogenic Belt: Journal of the Geological Society, v. 164, p. 31–47, https://doi.org/10.1144/0016-76492006-022.

Woelki, D., Regelous, M., Haase, K.M., Romer, R.H.W., and Beier, C., 2018, Petrogenesis of boninitic lavas from the Troodos Ophiolite, and comparison with Izu-Bonin-Mariana fore-arc crust: Earth and Planetary Science Letters, v. 498, p. 203–214, https://doi.org/10.1016/j.epsl.2018.06.041.

Xiao, W., Windley, B.F., Sun, S., Li, J., Huang, B., Han, C., Yuan, C., Sun, M., and Chen, H., 2015, A tale of amalgamation of three Permo-Triassic collage systems in Central Asia: Oroclines, sutures, and terminal accretion: Annual Review of Earth and Planetary Sciences, v. 43, p. 477–507, https://doi.org/10.1146/annurev-earth-060614-105254.

Xiao, W., Windley, B.F., Han, C., Liu, W., Wan, B., Zhang, J.E., Ao, S., Zhang, Z., and Song, D., 2018, Late Paleozoic to early Triassic multiple roll-back and oroclinal bending of the Mongolia collage in Central Asia: Earth-Science Reviews, v. 186, p. 94–128, https://doi.org/10.1016/j.earscirev.2017.09.020.

Yang, Y., Liang, C.Y., Zheng, C.Q., Xu, X.C., Zhou, X., and Hu, P.Y., 2022, The metamorphic characteristics of metapelites of the Mashan Group in Mashan area, eastern Heilongjiang Province, China: Constraint on the crustal evolution of the Jiamusi Massif: Gondwana Research, v. 102, p. 299–331, https://doi.org/10.1016/j.gr.2020.10.004.

Yi, Z.Y., and Meert, J.G., 2020, A closure of the Mongol-Okhotsk Ocean by the Middle Jurassic: Reconciliation of Paleomagnetic and geological evidence: Geophysical Research Letters, v. 47, https://doi.org/10.1029/2020GL088235.

Zabotkin, L.V., Baatar, T., and Biikhover, V.K., 1982, Report on 1:200,000-scale geological mapping and general prospecting in Dundgovi Province (sheet L-48-XXI): Ulaanbaatar, Mongolia, Geological Information Center, Open-File Report 3676.

Zhang, R.Y., Li, X.H., Yui, T.F., Jahn, B.M., Liou, J.G., and Ling, X.X., 2016, U-Pb geochronology of zircon and rutile from the Kokchetav metamorphic belt, northern Kazakhstan and its tectonic implications: European Journal of Mineralogy, v. 28, no. 6, p. 1203–1213, https://doi.org/10.1127/ejm/2016/0028-2523.

Zhao, P., Xu, B., and Jahn, B.M., 2017, The Mongol-Okhotsk Ocean subduction-related Permian peraluminous granites in northeastern Mongolia: Constraints from zircon U-Pb ages, whole-rock elemental and Sr-Nd-Hf isotopic compositions: Journal of Asian Earth Sciences, v. 144, p. 225–242, https://doi.org/10.1016/j.jseaes.2017.03.022.

Zhong, X.Y., and Li, Z.H., 2019, Forced subduction initiation at passive continental margins: Velocity-driven versus stress-driven: Geophysical Research Letters, v. 46, p. 11,054–11,064, https://doi.org/10.1029/2019GL084022.

Zhou, J.-B., Wilde, S.A., Zhao, G.-C., and Han, J., 2018a, Nature and assembly of microcontinental blocks within the Paleo-Asian Ocean: Earth-Science Reviews, v. 186, p. 76–93, https://doi.org/10.1016/j.earscirev.2017.01.012.

Zhou, X., et al., 2018b, Subduction initiation dynamics along a transform fault control trench curvature and ophiolite ages: Geology, v. 46, p. 607–610, https://doi.org/10.1130/G40154.1.

Zhou, X., Li, Z.H., Gerya, T.V., and Stern, R.J., 2020, Lateral propagation–induced subduction initiation at passive continental margins controlled by preexisting lithospheric weakness: Science Advances, v. 6, https://doi.org/10.1126/sciadv.aaz1048.

Zhu, M.S., Zhang, F.Q., Miao, L.C., Baatar, M., Anaad, C., Yang, S.H., and Li, X.B., 2016, Geochronology and geochemistry of the Triassic bimodal volcanic rocks and coeval A-type granites of the Olzit area, Middle Mongolia: Implications for the tectonic evolution of Mongol-Okhotsk Ocean: Journal of Asian Earth Sciences, v. 122, p. 41–57, https://doi.org/10.1016/j.jseaes.2016.03.001.

Zhu, M.S., Zhang, F.Q., Miao, L.C., Baatar, M., Anaad, C., Yang, S.H., and Li, X.B., 2018, The Late Carboniferous Khuhu Davaa ophiolite in northeastern Mongolia: Implications for the tectonic evolution of the Mongol-Okhotsk Ocean: Geological Journal, v. 53, p. 1263–1278, https://doi.org/10.1002/gj.2955.

Zhu, M.S., Pastor-Galán, D., Miao, L.C., Zhang, F.C., Ganbat, A., Li, S., Yang, S.H., and Wang, Z.L., 2023a, Evidence for early Pennsylvanian subduction initiation in the Mongol–Okhotsk Ocean from the Adaatsag ophiolite (Mongolia): Lithos, v. 436–437, https://doi.org/10.1016/j.lithos.2022.106951.

Zhu, M.S., Zhang, F., Smit, M.A., Pastor-Galan, D., Guilmette, C., Miao, L., Zou, Y., Yang, S.H., Ganbat, A., Tual, L., and Wang, Z.L., 2023b, Discovery of a >1,000 km Cambrian eclogite-bearing high-pressure metamorphic belt in the Central Asian Orogenic Belt: Implications for the final closure of the Pan-Rodinian Ocean: Journal of Geophysical Research: Solid Earth, v. 128, no. 1, https://doi.org/10.1029/2022JB025388.

Zhu, M.S., Wakabayashi, J., Pastor-Galán, D., Zhang, F.Q., Ganbat, A., Miao, L.C., Yang, S.H., and Wang, Z.L.,

2023c, Large-scale Permo-Triassic back-arc extensions of the Mongol-Okhotsk Ocean: Geological Society of America Bulletin, v. 135, p. 2563–2574, https://doi.org/10.1130/B36644.1.

Zhu, M.S., Yan, Z.Y., Pastor-Galan, D., Chen, L., Miao, L., Zhang, F., Li, S., and Yang, S.H., 2023d, Do microcontinents nucleate subduction initiation?: Geology, v. 51, p. 668–672, https://doi.org/10.1130/G51222.1.

Zhu, M.S., Zhang, F., Miao, L.C., Ganbat, A., Baatar, M., Anaad, C., Yang, S.H., and Wang, Z.L., 2023e, Permian-Triassic magmatic rocks in the Middle Gobi volcanic-plutonic belt, Mongolia: Revisiting the scissor-like closure model of the Mongol–Okhotsk Ocean: International Journal of Earth Sciences, v. 112, p. 741–763, https://doi.org/10.1007/s00531-022-02271-5.

Zhu, M.S., Pastor-Galán, D., Smit, M.A., Miao, L., Dong, M., Zhang, F., Sanchir, D., Ganbat, A., Liu, C., Luo, Y., and Li, S., 2024a, Ophiolites in the Central Asian Orogenic Belt record Cambrian subduction initiation processes: Communications Earth & Environment, v. 5, https://doi.org/10.1038/s43247-024-01905-7.

Zhu, M.S., Pastor-Galan, D., Smit, M.A., Sanchir, D., Zhang, F., Liu, C., and Miao, L., 2024b, The beginning of a Wilson cycle in an accretionary orogen: The Mongol–Okhotsk Ocean opened assisted by a Devonian mantle plume: Geophysical Research Letters, v. 51, https://doi.org/10.1029/2024GL109028.

Zorin, Y.A., 1999, Geodynamics of the western part of the Mongolia–Okhotsk collisional belt, Trans-Baikal region (Russia) and Mongolia: Tectonophysics, v. 306, p. 33–56, https://doi.org/10.1016/S0040-1951(99)00042-6.

Science Editor: Mihai Ducea
Associate Editor: Dongfang Song

Manuscript Received 21 October 2025
Revised Manuscript Received 1 March 2026
Manuscript Accepted 4 May 2026